

Right- and left-loop short shRNAs have distinct and unusual mechanisms of gene silencing

Anne Dallas¹, Heini Ilves¹, Qing Ge¹, Pavan Kumar¹, Joshua Shorestein¹, Sergei A. Kazakov¹, Trinna L. Cuellar², Michael T. McManus^{2,3,4}, Mark A. Behlke⁵ and Brian H. Johnston^{1,6,*}

¹SomaGenics, Inc., 2161 Delaware Avenue, Santa Cruz, CA 95060, ²UCSF Diabetes Center, ³Department of Microbiology and Immunology, ⁴WM Keck Center for Noncoding RNAs, UCSF, San Francisco, CA 94143, ⁵Integrated DNA Technologies, Inc., Coralville, IA 52241 and ⁶Department of Pediatrics, Stanford University School of Medicine, Stanford, CA 94305, USA

Received November 18, 2011; Revised June 10, 2012; Accepted June 14, 2012

ABSTRACT

Small hairpin RNAs (shRNAs) having duplex lengths of 25–29 bp are normally processed by Dicer into short interfering RNAs (siRNAs) before incorporation into the RNA-induced silencing complex (RISC). However, shRNAs of ≤ 19 bp [short shRNAs (sshRNAs)] are too short for Dicer to excise their loops, raising questions about their mechanism of action. sshRNAs are designated as L-type or R-type according to whether the loop is positioned 3' or 5' to the guide sequence, respectively. Using nucleotide modifications that inhibit RNA cleavage, we show that R- but not L-sshRNAs require loop cleavage for optimum activity. Passenger-arm slicing was found to be important for optimal functioning of L-sshRNAs but much less important for R-sshRNAs that have a cleavable loop. R-sshRNAs could be immunoprecipitated by antibodies to Argonaute-1 (Ago1); complexes with Ago1 contained both intact and loop-cleaved sshRNAs. In contrast, L-sshRNAs were immunoprecipitated with either Ago1 or Ago2 and were predominantly sliced in the passenger arm of the hairpin. However, 'pre-sliced' L-sshRNAs were inactive. We conclude that active L-sshRNAs depend on slicing of the passenger arm to facilitate opening of the duplex, whereas R-sshRNAs primarily act via loop cleavage to generate a 5'-phosphate at the 5'-end of the guide strand.

INTRODUCTION

RNA interference (RNAi) is a naturally occurring mode of post-transcriptional gene regulation that has broad potential applications in both research and therapeutic settings. It is the process by which many genes are regulated by microRNAs (miRNAs), and it is through RNAi that exogenous double-stranded RNAs (dsRNA), including short interfering RNAs (siRNAs) and small hairpin RNAs (shRNAs) can induce degradation of sequence-matching target RNAs (1,2). A central step in the process involves the association of dsRNAs with an Argonaute (Ago) protein in the RNA-induced silencing complex (RISC), with subsequent removal of one RNA strand (the passenger strand). These two steps have been termed RISC loading and RISC activation, respectively (2,3). However, the roles of the various members of the Ago family as well as several other proteins associated with RISC in mediating the effects of pre-miRNAs, siRNAs and shRNAs remain incompletely understood despite extensive *in vitro* and *in vivo* studies in a variety of model systems. It has become clear that there are significant differences in the RNAi process in different classes of organisms, and in the present work we have focused on the human system.

The nature of the cellular RNAi response depends on the length of the triggering dsRNA. RNAs containing duplexes longer than 24 bp, including most pre-miRNAs, long shRNAs (lshRNAs) and long dsRNAs, are first processed by the RNase III-family endonuclease Dicer (4–6) into ~ 19 –21 bp RNAs containing 5'-monophosphates, 3'-hydroxyl groups and 3'-dinucleotide overhangs (7).

*To whom correspondence should be addressed. Tel: +1 831 426 7700; Fax: +1 831 420 0685; Email: bjohnston@somagenics.com
Present addresses:

Qing Ge, Department of Immunology, Peking University Health Science Center, Beijing 100191, China.

Pavan Kumar, Eisai, 4 Corporate Drive, Andover MA 01810, USA.

Joshua Shorestein, Department of Chemistry and Biochemistry, University of Colorado at Boulder, Boulder, CO 80309, USA.

Trinna L. Cuellar, Genentech Inc., 1 DNA Way, South San Francisco, CA 94080, USA.

dsRNAs that have shorter duplexes, such as siRNAs, short shRNAs (sshRNAs) (8,9) and the recently characterized pre-miR-451 (10,11), are not processed by Dicer, and its role in loading these molecules into RISC in humans has been the subject of much study and debate. Previously, it was reported that a RISC-loading complex (RLC) comprising Dicer, TAR-RNA binding protein (TRBP) and Argonaute-2 (Ago2) loads siRNAs and miRNAs onto Ago2 (12–15). However, it has also been shown that pre-miRNAs can bind directly to Ago2 in the absence of Dicer (16), and RNAi-mediated gene silencing by exogenously-added siRNAs occurs in Dicer-knockout cell lines (17,18). Recently, a Dicer-independent pathway of RISC activation was inferred from *in vitro* reconstitution studies that showed that RISC activation could occur by interaction of siRNAs with Ago2 and C3PO in the absence of Dicer-TRBP (19). In addition, a study of the biogenesis of a miR-451, a miRNA whose pre-miRNA form consists of a fully-paired stem-loop of <19 bp, found that mature miR-451 was generated by cleavage of the pre-miRNA by Ago2 without prior processing by Dicer (10,11). These studies support the view that dicing (processing by Dicer) can be decoupled from RISC loading and activation.

In any case, to activate RISC, a short dsRNA must be unwound, with retention of one strand, the guide strand, bound to Ago in unpaired form. Guide strand selection of siRNAs and diced miRNAs is thought to be governed by the asymmetric thermodynamic profile of the duplex (20,21). In a recent study, it was shown that Dicer might act also to facilitate orientation of siRNAs such that the proper strand is selected to be the guide strand in active RISC through interaction with the helicase domain of Dicer (22). All mammalian RISC complexes contain one of the four Ago proteins, each of which have characteristic N-terminal, PAZ, middle (MID) and PIWI domains (23). Depending on which Ago is present in the RISC complex, different pathways of silencing can occur. The PIWI domain of Ago2, which has an RNase H-like structure (24–26), catalyzes the cleavage or ‘slicing’ of the phosphodiester linkage of complementary RNAs opposite nucleotide 10/11 from the 5′-end of the guide strand (27–30). In crystal structures of Ago proteins and their complexes, the 5′-phosphate group of the guide strand is buried in a pocket of the MID domain (31–35) while the 3′-end is anchored by the PAZ domain (36,37). This arrangement allows for precise alignment of the cleavage site of the target RNA with the active site of the PIWI domain. Despite a high degree of sequence conservation among this family, only Ago2 has target-slicing activity whereas Ago1, Ago3 and Ago4 induce translational repression by other mechanisms (38,39). In contrast to *Drosophila*, where perfectly Watson–Crick paired duplexes and duplexes containing mismatches are sorted, respectively, into Ago2- and Ago1-containing RISCs (40), in mammals both perfect and mismatched duplexes can associate with all four Ago proteins (28,41–43).

In addition to catalyzing cleavage of target RNAs, Ago2 has been shown to slice the passenger strand of bound siRNAs (44,45) and pre-miRNAs (46), facilitating its subsequent degradation by another endonuclease, C3PO (19,47,48). Wang *et al.* (42) found that Ago1 also

cleaved the passenger strand *in vitro* despite not being able to cleave target RNA. However, in a subsequent study, it was reported that the passenger strand was not readily dissociated from Ago1-containing RISC complexes (49). When the passenger strand cleavage site is blocked by chemical modification or by mismatches between the two strands of the siRNA, a slower ‘bypass’ pathway dissociates and destroys the passenger strand, possibly via the ATP-dependent RNA helicase A, liberating the mature RISC (44,50–54). Thus, multiple pathways appear to be available for RISC activation. Once formed, the activated RISC containing the single-stranded guide strand can then initiate gene silencing by base pairing of its seed sequence (nucleotides 2–8) with the target, as can be seen in crystal structures of the guide-strand-containing argonaute-silencing complex (32–35).

Several groups including ours have reported a unique class of synthetic, short shRNAs, sshRNAs, whose efficacy is as good as or, in some cases, better than siRNAs that target the same sequences (8,9,55–57). We have shown that these sshRNAs are extremely potent, with IC₅₀s in the low-picomolar range, and they are of interest for development as therapeutic agents (8). sshRNAs typically have a stem of 19 bp but may be as short as 16–17 bp, with a connecting sequence between the guide and passenger sequences (or arms) ranging in length from 0 (i.e. direct connection of guide and passenger sequences) to 10 nt (8). Hereafter, we refer to this connecting sequence as a ‘linker’ without regard to its secondary structure, and we use the term ‘loop’ to refer to the nominally unpaired region between the two arms of an sshRNA without regard to whether it exactly corresponds to the linker. (Thus, an sshRNA may lack a linker but still have a loop comprised of nucleotides from the guide and/or passenger strands.) Compared to shRNAs having a longer duplex stem, sshRNAs are unique on several accounts. Whereas shRNAs of 21 bp or longer (lshRNAs) can be Dicer substrates, it has been shown that sshRNAs are not cleaved by Dicer *in vitro* (6,8,9,58). At the same time, results of 5′-RACE (rapid amplification of cDNA ends) analysis indicated that target suppression by sshRNA occurs via RNAi-mediated messenger RNA cleavage (8). Thus, how sshRNAs are processed to facilitate RISC loading and subsequent activation has been an open question. Unlike lshRNAs, which are converted to siRNAs prior to or during RISC-loading, sshRNAs have an intrinsic ‘handedness’ to them because the guide sequence arm can be positioned either 5′ of the linker (left-hand type or L-type) or 3′ to the linker (right-hand type or R-type) (8,57). We have observed differing activities for sshRNAs that target the same sequence depending on whether they are L-type or R-type. L- and R-sshRNAs also have different structural requirements for activity. For example, the 3′ overhang of L-sshRNAs can be deleted with little or no activity loss, but is required for optimal performance of R-sshRNAs (8). Due to these differences in structure requirements for silencing activity of L- versus R-sshRNAs, we were prompted to investigate the mechanism of how these sshRNAs are used by the RNAi machinery to exert their distinct functionalities. We find that sshRNAs can be

processed differently by the RNAi machinery depending on the length of the linker and whether they are L- or R-type. These findings underscore the multiplicity of pathways available to dsRNAs for gene silencing.

MATERIALS AND METHODS

Preparation of shRNAs and sshRNAs

Synthetic, HPLC-purified sshRNAs were obtained from Integrated DNA Technologies (IDT, Coralville, IA) and resuspended in RNase- and pyrogen-free buffer containing 20 mM KCl, 6 mM HEPES-KOH (pH 7.5), 0.2 mM MgCl₂ (Thermo Fisher Scientific, Dharmacon Products, Lafayette, CO). sh1 was obtained from Thermo Fisher Scientific. After resuspension, sshRNAs were heated to 95°C for 4 min and snap-cooled in an ice-water bath for 20 min to eliminate dimers (8). All sshRNAs used in these studies were confirmed to be in monomeric hairpin form by non-denaturing PAGE. The sequences of all the sshRNAs used in this article are presented in Supplementary Table S1. DNA oligonucleotides were purchased from IDT.

Reporter gene assays

The human kidney cell line 293FT (Invitrogen, Carlsbad, CA) was maintained in DMEM (Cambrex, Walkersville, IN) with 10% fetal bovine serum (Hyclone, Logan, UT), supplemented with 2 mM L-glutamine and 1 mM sodium pyruvate. One day prior to transfection, cells were seeded at 23 000 cells/well in a 96-well plate, resulting in ~80% cell confluency at the time of transfection. Transfections were performed using Lipofectamine 2000 (Invitrogen) following the manufacturer's instructions. 13 ng of IRES/fLuc, 20 ng pSEAP2 (a transfection control plasmid) (BD Biosciences Clontech, San Jose, CA) and the indicated amounts of shRNAs were cotransfected into 293FT cells. IRES/fLuc is a dual luciferase expression plasmid in which the entire hepatitis C virus (HCV) internal ribosome entry site (IRES) is placed between the coding sequences for the *Renilla* and *firefly* luciferases (rLuc and fLuc, respectively) so that fLuc expression is dependent on the IRES, to which RNAi inhibitors are targeted. Forty-eight hours after transfection, the cells were lysed and luciferase activity was measured in a MicroLumat LB 96P luminometer (Berthold Technologies, Bad Wildbad, Germany). Unless otherwise indicated, all the siRNA and shRNA samples were tested in triplicate and two or more independent experiments were performed. Percent silencing was calculated relative to cells transfected with the reporter plasmid in the absence of any RNAi agent. Similar transfection conditions were used when a second luciferase reporter construct, psiCHECKTM-2-pIRES was tested. The latter was constructed from plasmid psiCHECKTM-2 (Promega, Madison, WI) by inserting a fragment of the HCV IRES (pIRES, the targeting sequence for all the si/shRNAs involved in this study) at the 3'-end of rLuc by site-directed mutagenesis. For each siRNA or shRNA transfection, the expression of rLuc was normalized to its corresponding *firefly* expression.

Dicer knockout cells

Conditional Dicer knockout mouse embryonic fibroblasts [CDK-MEFs, described in (16)] were maintained in DMEM (Cambrex) with 10% fetal bovine serum (Hyclone), supplemented with 2 mM of L-glutamine and 1 mM of sodium pyruvate. Recombinant adenoviral stocks (Adeno-Cre, Ad5CMVCre) were purchased from the Gene Transfer Vector Core facility of the University of Iowa College of Medicine (Iowa City, IA). To induce the depletion of Dicer by recombination at loxP sites, cells were first resuspended in serum-free DMEM to a final concentration of 1×10^7 cells/ml. Then, 6×10^7 plaque-forming units (pfu) of Adeno-Cre were added to infect 7×10^5 cells by incubating at 37°C for 1 h with gentle shaking (~86 pfu/cell). After 1 h, cells were pelleted at 1400 g for 3 min and the supernatant was removed. Cells were resuspended in complete DMEM and seeded at 3.5×10^6 cells/well in a 6-well plate. The MEFs were cultured for an additional 7 days, and the level of recombination was determined by measuring YFP expression with flow cytometry every 2–3 days (FACScan, Becton Dickinson).

CDK-MEF transfections

One day prior to transfection, CDK-MEFs with and without prior Adeno-Cre treatment were seeded at 10 000 cells/well in 96-well plate, resulting in ~80% cell confluency at the time of transfection. Plasmid and shRNA/siRNA transfections were performed using TransIT-LT1 and TransIT-TKO reagents (Mirus), respectively, following the manufacturer's protocol. Eighty nanograms of IRES/fLuc reporter plasmid and various amounts of shRNA or siRNA were cotransfected into CDK-MEFs. Plates were subjected to centrifugation ('spinoculation') at 425g for 10 min at 25°C. After spinoculation, the plates were placed back in the incubator. Forty-eight hours later, the cells were lysed, and luciferase activity was assayed as described above.

Mapping of RNA target cleavage sites by 5'-RACE analysis

293FT cells were transfected with siRNA or sshRNA together with pSG154m target expression plasmid as described above. Total RNA was extracted 12h post-transfection and mRNA was purified using the Oligotex mRNA kit (Qiagen, Germantown, MD). The mRNA was then subjected to 5'-RACE analysis using the GeneRacer Kit (Invitrogen) following the manufacturer's instructions with the following modifications. The GeneRacer RNA adaptor was ligated to mRNAs at their 5'-ends. Ligated RNAs were reverse transcribed using the primer 5'-CGCG CCCAACACCGGCATAAAGAATT-3' and amplified by PCR using primers 5'-GCTTCTGCCAACCGAACG GACATTT-3' and (adaptor specific) 5'-CGACTGGAGC ACGAGGACTGA-3'. PCR was started with 5 cycles of 95°C for 45 s and 72°C for 30 s, followed by 5 cycles of 95°C for 45 s and 69°C for 30 s, and finally 25 cycles of 95°C for 45 s, 65°C for 30 s and 72°C for 30 s. The PCR products were analyzed on a 2% agarose gel and the band

with the predicted length of the cleavage product was excised, purified, cloned and sequenced (Retrogen).

Ago2 and Ago1 immunoprecipitations

One day before transfection, 1.8×10^6 293FT cells were seeded in T25 tissue culture flasks. sshRNAs were ^{32}P -labeled at either the 5'- or 3'-end and then transfected into 293FT cells at 4–10 nM final concentration. For immunoprecipitation of Ago2 and Ago1 complexes, cells were lysed at 6 h after transfection. To isolate the RNAs from the Ago2-bound complexes, the cell lysates were incubated with bead-coupled monoclonal anti-human Ago2 antibody (Wako, clone 4G8) overnight at 4°C with rotation and purified following the manufacturer's protocol (Human Ago2, MicroRNA Isolation Kit, Wako Chemicals). A 200- μl aliquot of the supernatant out of a total of 1 ml from the incubation with hAgo2-antibody beads was saved for further analysis. These supernatants were phenol–chloroform extracted and concentrated by ethanol precipitation. For immunoprecipitation of Ago1 complexes, lysates were incubated with anti-hAgo1 antibody (Wako, clone 2A7) that was pre-coupled to Protein G Dynabeads (Invitrogen). The magnetic bead-captured complexes were washed extensively and eluted as was done with the Ago2-bound complexes. A 200- μl fraction of the supernatant (out of 1 ml) was saved and processed as described above for the Ago2 immunoprecipitations for further analysis. RNAs that were isolated from antibody-bound complexes or extracted from supernatants were then analyzed by denaturing 12% PAGE (8 M urea/20% formamide).

RESULTS AND DISCUSSION

Evidence for Dicer-independent activity of sshRNA in cells

In a prior study, we showed that neither L- nor R-type sshRNAs were cleaved by Dicer in cell-free systems (8), consistent with results obtained by Siolas *et al.* (9). To see if this is also the case in cells, we compared the efficacy of sshRNAs in cells with and without Dicer function. Engineered MEFs whose Dicer genes were flanked by loxP sites and which contained a Cre-conditional yellow fluorescent protein (YFP) reporter were treated with an adenovirus expressing the Cre recombinase (Ad–Cre) (16). Upon Cre expression, Dicer was excised and YFP was expressed. In this experiment, it was important that the testing of sshRNA efficacy in the presence and absence of Dicer be timed to take place after most residual Dicer protein had decayed following Ad–Cre treatment, but before any *dicer*^{+/+} cells that escaped transduction had time to outgrow the *dicer*^{-/-} cells, which grow more slowly. Flow cytometer analysis 7 days post-adenoviral infection showed that 95% of cells expressed YFP and had therefore lost both *dicer* alleles (Supplementary Figure S1A). Western blot analysis confirmed that endogenous Dicer protein was depleted by 48 h following Ad–Cre treatment (Supplementary Figure S1B). As a further measure of the depletion of Dicer protein from the cells, we confirmed by RT-qPCR analysis that several mature endogenous miRNAs were depleted 7

days after Ad–Cre treatment (Supplementary Figure S1C) (59).

Choosing the Day-7 time point for testing sshRNA efficacy under Dicer-depleted conditions, we transfected the cells with the reporter plasmid pSG154m, in which fLuc expression is dependent on the hepatitis C virus (HCV) internal ribosome entry site, together with various concentrations of the sshRNAs and siRNA to be tested (Figure 1A). Silencing activity was determined by measuring luciferase levels in cells transfected with RNAi inhibitors relative to cells transfected with only the reporter plasmid. As expected, upon transfecting *dicer*^{+/+} or *dicer*^{-/-} cells with siRNA 19-3 (Figure 1B), a molecule whose structure and termini correspond to typical products of Dicer processing, we observed no change in silencing activity, similar to what has been observed with other Dicer knockout cell lines (17,18). SG224(L), a highly-active sshRNA having the same target site as si-19-3 [previously characterized in (60)], also showed very little loss of activity in the *dicer*^{+/+} compared with *dicer*^{-/-} cells, suggesting that cleavage of sshRNAs by Dicer is not required for target-silencing activity in cells (Figure 1B). Transfected SG221C, a scrambled control sshRNA, did not silence the luciferase target RNA under these conditions, indicating that silencing activity was indeed specific (Figure 1B). To be sure that the specific silencing was not due to the formation of dimers that could be Dicer substrates (by virtue of their longer duplex length), we used an sshRNA having 2'-OMe modifications on its passenger arm and loop that cannot be cleaved by Dicer *in vitro* in either its monomer (hairpin) or dimer (extended duplex) forms (Supplementary Figure S2). The unmodified form of this sshRNAs [SG105(L), Supplementary Table S1], can be cleaved *in vitro* by Dicer in its dimer but not its hairpin monomer form, as shown in Supplementary Figure S2. Since Dicer is thought to act as a 'molecular ruler' based on its crystal structure (61), producing siRNAs that are 21–23 nt long, the inability of Dicer to cleave sshRNAs that are shorter than 21–23 nt *in vitro*, coupled with the lack of any reduction in silencing activity in Dicer-depleted cells, strongly suggests that the silencing activity of sshRNAs is not dependent on Dicer. This result provides further support for the decoupling of Dicer activity with RISC activation, as has been proposed first in *Drosophila* (62–64) and later in humans (19,43). Interestingly, the activity of sh1, an shRNA with a 25-bp stem and a 10-nt linker (Figure 1B) that is known to be a substrate for Dicer *in vitro* (8) was also unaffected by depletion of Dicer, consistent with evidence for direct interaction of this molecule with Ago2 as described below. This observation is also consistent with the results of Yoda *et al.* (43), who observed that a hairpin pre-miRNA of similar length could induce target cleavage with recombinant Ago2 in a cell-free system in the absence of any dicing activity.

R- but not L-sshRNAs require loop cleavage for optimum activity

If Dicer does not excise the loop of sshRNAs, we next wondered if an alternative nuclease, perhaps single-strand specific, cleaves the loop and allows the resulting two

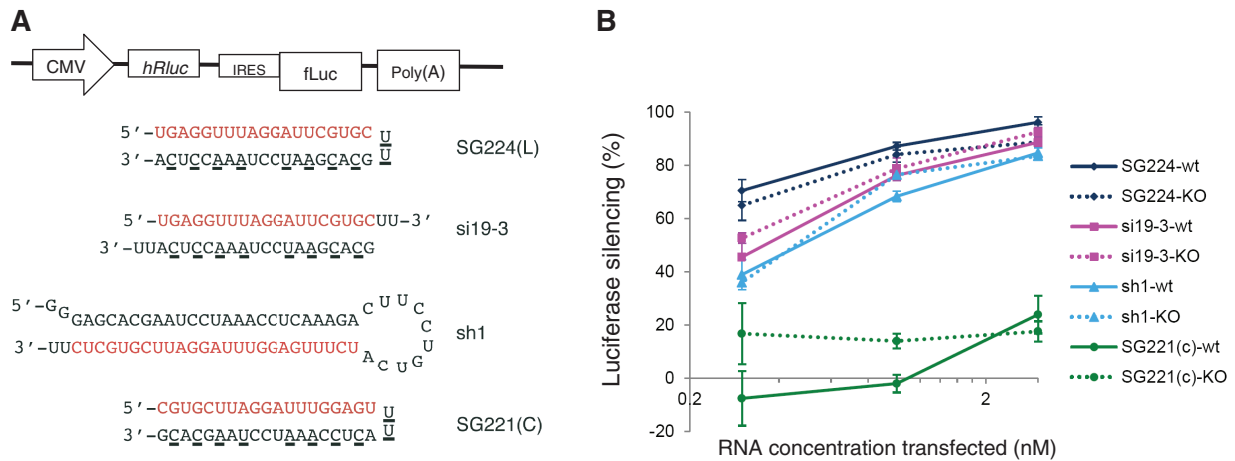


Figure 1. Depletion of Dicer has no effect on sshRNA activity. (A) Diagram of the IRES/fLuc reporter construct. fLuc expression is driven by the HCV IRES (top). Sequences and putative secondary structures of RNA molecules transfected into CDK-MEFs are shown below. The guide strands are highlighted in red text. Nucleotides that are underlined contain 2'-O-Me-modifications. (B) RNAs in (A) were co-transfected with target plasmid into CDK-MEFs that were not treated (solid lines) or 7 days after induced recombination by Adeno-Cre to knock out the *dicer* alleles (dotted lines). Percent silencing was calculated by normalizing to luciferase reporter expression levels 48 h after transfection.

strands of the duplex to act as an siRNA. One such RNase, MCPIP1, which cleaves terminal loops of precursor miRNAs, has been recently described (65). We have previously reported that L-sshRNAs (Figure 2A) featuring a dinucleotide (UU) linker connecting 19-nt guide and passenger sequences are potent gene silencing inhibitors (8). One such L-sshRNA, SG105(L) (Figure 2E, Supplementary Table S1), has potency similar to the corresponding siRNA si19-3 (Figure 2B). Because the nucleotides flanking the linker are a C and a G (Supplementary Table S1), this molecule conforms to the class of canonical ultrastable tetraloops having the sequence CUUG [nucleotides 19–22 of SG105(L)] (66). While commonly referred to as a tetraloop, solution NMR studies showed that the first and last nucleotides of this loop form a C–G Watson–Crick pair, leaving only the two U residues unpaired (67). If the mechanism of action involves cleavage of the linker to create a guide strand with a 3'-OH, cleavage could be expected before or after one of these nucleotides. To test whether such cleavage is essential to the function of L-sshRNAs, RNase-resistant 2'-deoxy (DNA) and phosphorothioate (PS) modifications were introduced into the linker [SG209(L): DNA substitution at nucleotides 19–22; SG210(L): DNA at nucleotides 19–22 + PS after nucleotides 18–22] (Supplementary Table S1). As shown in Figure 2B, no loss of activity was seen with these linker-modified L-sshRNAs. Replacing the entire UU linker of SG105 with a non-nucleotide linker [producing SG229(L)] also had no effect on activity (Supplementary Figure S3A). These results indicate that the linker of L-sshRNAs does not need to be cleaved to enable target knockdown.

For R-sshRNAs, which have the guide sequence at the 3'-end of the hairpin (Figure 2A), the linker would need to be cleaved in a precise manner if it is to expose the 5'-phosphate of the first nucleotide of the guide strand. Siolas *et al.* (9) detected two distinct small RNAs of 21 and 23 nt after transfecting a 19-bp R-type shRNA with a

4-nt linker (5'-CCAA-3') into cells. They suggested that the 19-bp shRNA might be cleaved at the loop before or after entering into RISC by a single-strand-specific ribonuclease other than Dicer. To test this, we modified the 5-nt linker of an R-sshRNA [SG68(R)] by introducing 2'-deoxynucleotides and PS linkages to inhibit cleavage by ribonucleases. Unlike with the L-sshRNAs, the potency of this modified R-sshRNA [SG234(R)] was significantly reduced compared to the unmodified SG68(R) (Figure 2C). Similarly, when the 2-nt linker of the R-type molecule SG150(R) was modified by 2'-OMe groups to form SG257(R), potency also suffered (Supplementary Figure S3B). Although we have not formally excluded the possibility that these chemical modifications block binding of R- but not L-sshRNAs to Ago2, these results suggest that a loop that is susceptible to cleavage by endonucleases is necessary for the optimal activity of R-sshRNAs.

To examine this question further in a different target sequence context, we compared the efficacy of chemically-unmodified R- and L-sshRNA with either 2- or 5-nt linker sequences. R- and L-sshRNAs with 5-nt linkers (SG74R and SG74L) had similar activity to each other and to the analogous L-type with a 2-nt linker, but when the linker of the R-type was reduced to 2 nt, efficacy dropped sharply (Figure 2D). Since sshRNAs with 2-nt linkers are much more resistant to RNase cleavage than 5-nt linkers even when they do not belong to a class of ultrastable tetraloop sequences (60) (Supplementary Figure S4), these results additionally support a silencing mechanism in which loop cleavage is particularly important for R-sshRNAs.

R- but not L-sshRNAs require loop cleavage for accurate target cleavage

To investigate further whether loop cleavage is necessary for function of R-sshRNAs, we used 5'-RACE analysis to determine the site of target cleavage for a series of

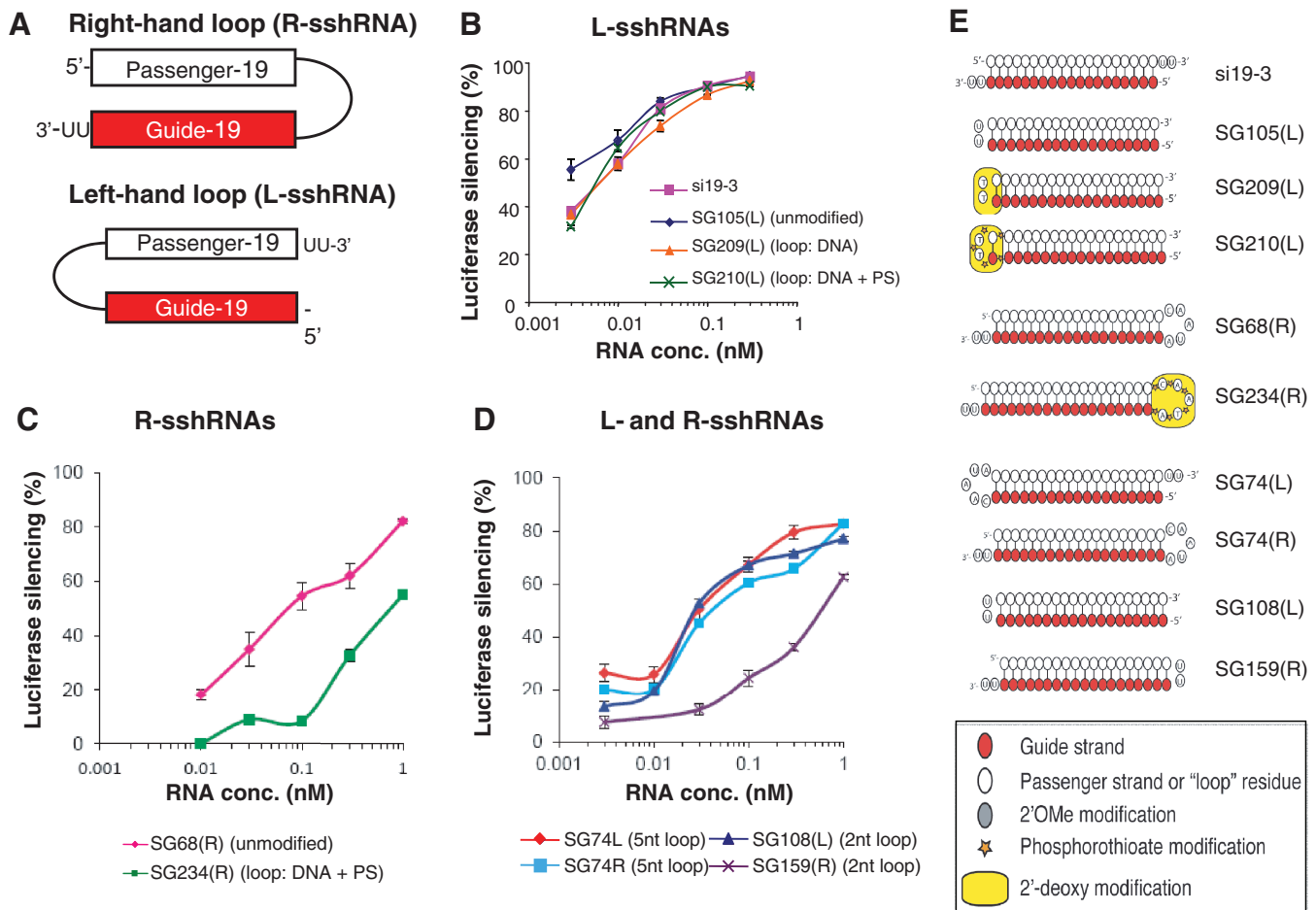


Figure 2. Comparison of L- and R-sshRNAs with various linker lengths and chemical modifications. (A) Schematic of R- and L-sshRNA configurations. (B–D) sshRNAs against the same target were compared for their ability to suppress the expression of the HCV IRES/fLuc reporter in 293FT cells. The sshRNAs were cotransfected in triplicate with the reporter DNA. si19-3, which is specific for the same target gene, was used as a positive control. (B) Effect of various linker (loop) modifications on the activity of L-sshRNAs. (C) Effect of various linker modifications on the activity of R-sshRNAs. (D) Effect of linker size on the activity of L- and R-sshRNAs (E) Schematic cartoons of the sshRNAs in this study, showing guide sequences (red ovals), passenger and linker sequences (white ovals), 2'-deoxy substitutions (yellow highlights) and phosphorothioate modifications (stars).

modified and unmodified R- and L-sshRNAs as well as an siRNA, all targeting the same site on an IRES-fLuc mRNA (Figure 3). Based on the frequency with which particular termini appeared upon cloning and sequencing of 5'-RACE products, siRNAs produced cleavage only at the predicted slicing site, opposite to nucleotide 10/11 from the 5'-end of the siRNA (5 out of 5 clones). Of the L-sshRNAs, most cleavage (16 of 21 clones) occurred at the predicted slicing site whether or not the linker was modified to make it nuclease resistant. However, in the case of R-sshRNAs, the proportion of cleavage occurring at the predicted site was much lower and depended on the susceptibility of the linker to nuclease cleavage. SG68(R), with an unmodified 5-nt loop, produced the predicted target cleavage in 2 out of 3 clones sequenced. SG150(R), with an unmodified 2-nt linker, cleaved the target at the predicted site for 5 out of 10 clones, at a site 2 nt 3' to that site for 2 clones of the 10, and further downstream for the other 2 clones. For SG234(R), which had nuclease-resistant modifications to its 5-nt linker, only

1 out of 7 clones showed cleavage at the predicted site. The other 6 clones showed cleavage both upstream and downstream of the predicted site, scattered over a 67-nt span of sequence. These results again strongly suggest that cleavage of the linker sequence in R-sshRNAs, resulting in a terminal phosphate group at the 5'-end of the antisense sequence, is required for normal target slicing action. However, target cleavage may occur in an inefficient and inaccurate manner in the absence of loop cleavage.

Passenger-strand slicing: L- versus R-sshRNAs

siRNAs and pre-miRNA duplexes initially bind to Ago2 as largely double-stranded molecules. Once bound to Ago2, the passenger strand is sliced opposite nucleotide 10/11, which leads to its removal. To investigate whether similar passenger strand (or arm) slicing also occurs with sshRNAs, chemical modification of the passenger sequence was employed to look for effects on activity.

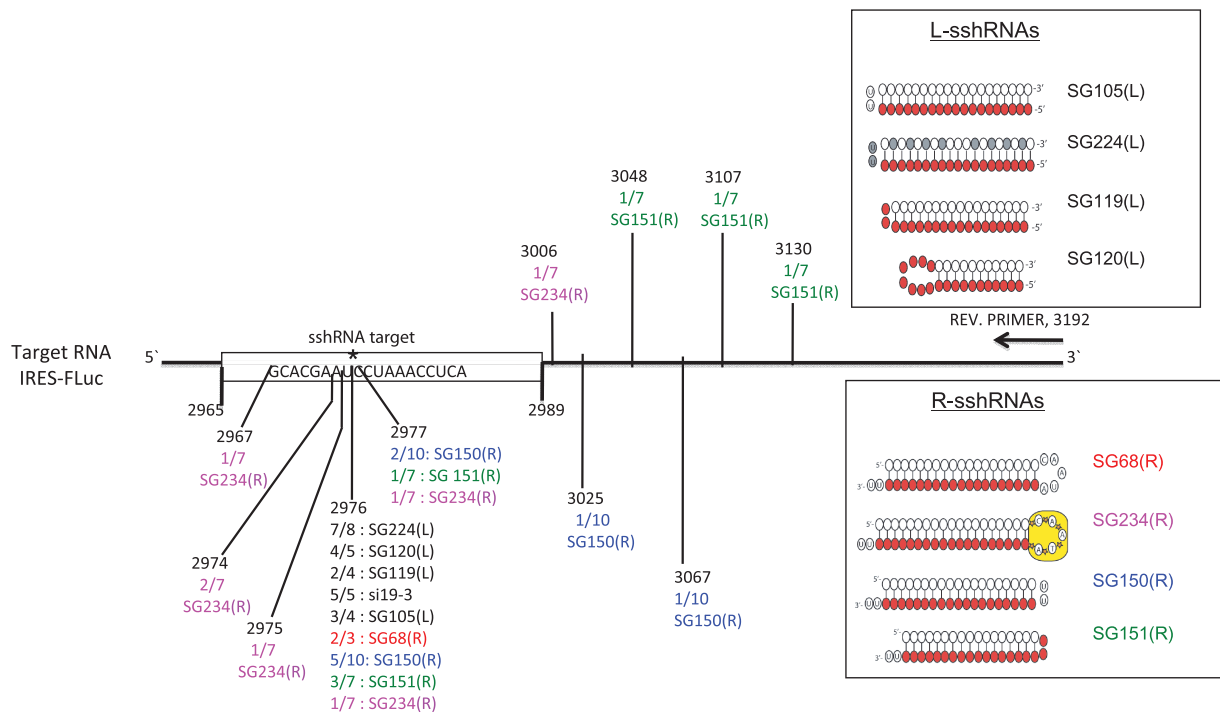


Figure 3. Influence of sshRNA structural features and modification on positions of target cleavage. A diagrammatic representation of the portion of interest of the target mRNA is shown indicating the sshRNA target site (nucleotides 2965–2989) and the priming position of the reverse primer used for 5'-RACE. The various cleavage sites (and the number of clones out of the total sequenced obtained for each) for all the sshRNAs used in this study are indicated. All L-sshRNAs are labeled in black. All R-sshRNAs are labeled in color. The predicted cleavage site by Ago2 is marked by an asterisk. Schematic cartoons describe the sshRNAs constructs in this figure. Key: guide strand (red ovals), passenger strand and linker sequences (white ovals), 2'-O-methyl modifications (gray ovals), 2'-deoxy substitutions (yellow highlight), phosphorothioate modifications (stars).

A significant activity loss was found when a 2'-O-methyl group was placed on the passenger-arm nucleotide opposite position 11 in addition to a single PS bond between the passenger-strand nucleotides opposite positions 10/11 of the guide arm [11-Me + PS, SG222(L)] (Figure 4A). Thus, modifications to the passenger arm of L-sshRNAs that reduce susceptibility to slicing also reduce silencing activity. Since R-sshRNAs with 2-nt linkers have impaired activity, we tested the effect of modifying the slicer site of the passenger strand on silencing activity for R-sshRNAs with 5-nt linkers. Unlike with L-sshRNAs, when the 11-Me + PS passenger-strand modifications were introduced into an R-sshRNA [SG230(R)], there was no change in silencing activity (Figure 4B).

When the linker sequence of an R-sshRNA is reduced in size or modified to render it less cleavable, its activity is significantly reduced (Figure 2D and Supplementary Figure S3B). On the other hand, linker cleavability of L-sshRNAs has no bearing on their efficacy (Figure 2B and Supplementary Figure S3A). These results suggest that active R-sshRNAs depend on loop cleavage while L-sshRNAs depend more on passenger-strand slicing. Further support for this hypothesis comes from examination of sshRNAs having 4-nt mismatches at the center of the sense sequence. The L mismatched version [SG145(L)] lost all activity, as was also the case when the entire sense sequence was substituted with deoxyribonucleotides (SG227) (Figure 4A). However, the activity of a similarly mismatched R-sshRNA was only partially reduced

(Figure 4B), suggesting that mismatches in the L-sshRNA disable its silencing activity not by blocking Ago binding (which would presumably apply to both R- and L-forms) but rather by blocking passenger-arm slicing. To more carefully address the question of why R- and L-sshRNAs appear to have different requirements for passenger-strand slicing, we undertook a study of RNAs that could be immunoprecipitated from cell lysates by anti-Ago antibodies, as described below.

Stable binding of sshRNAs to hAgo2

Considering the findings that the linker of an L-sshRNA need not be cleaved during RNAi and that blocking passenger-arm slicing reduces efficacy, we hypothesized that full-length L-sshRNA is bound by Ago2 without any prior processing. RISC activation could then be accomplished by slicing of the passenger arm by Ago2 and degradation of the resulting 3' fragment of ~10 nt by C3PO (19,47) in a Dicer-independent manner. In this scenario, two RNA products might be found in association with Ago2: a full-length hairpin and a fragment comprising the guide sequence, linker, and half of the passenger arm. Indeed, in Ago2 pull-down experiments, two complexes were immunoprecipitated from cell extracts with a hAgo2 antibody after the cells were transfected with the 40-nt, 5'-end labeled L-sshRNA SG224. Denaturing PAGE analysis showed that these fragments had electrophoretic mobilities corresponding to the

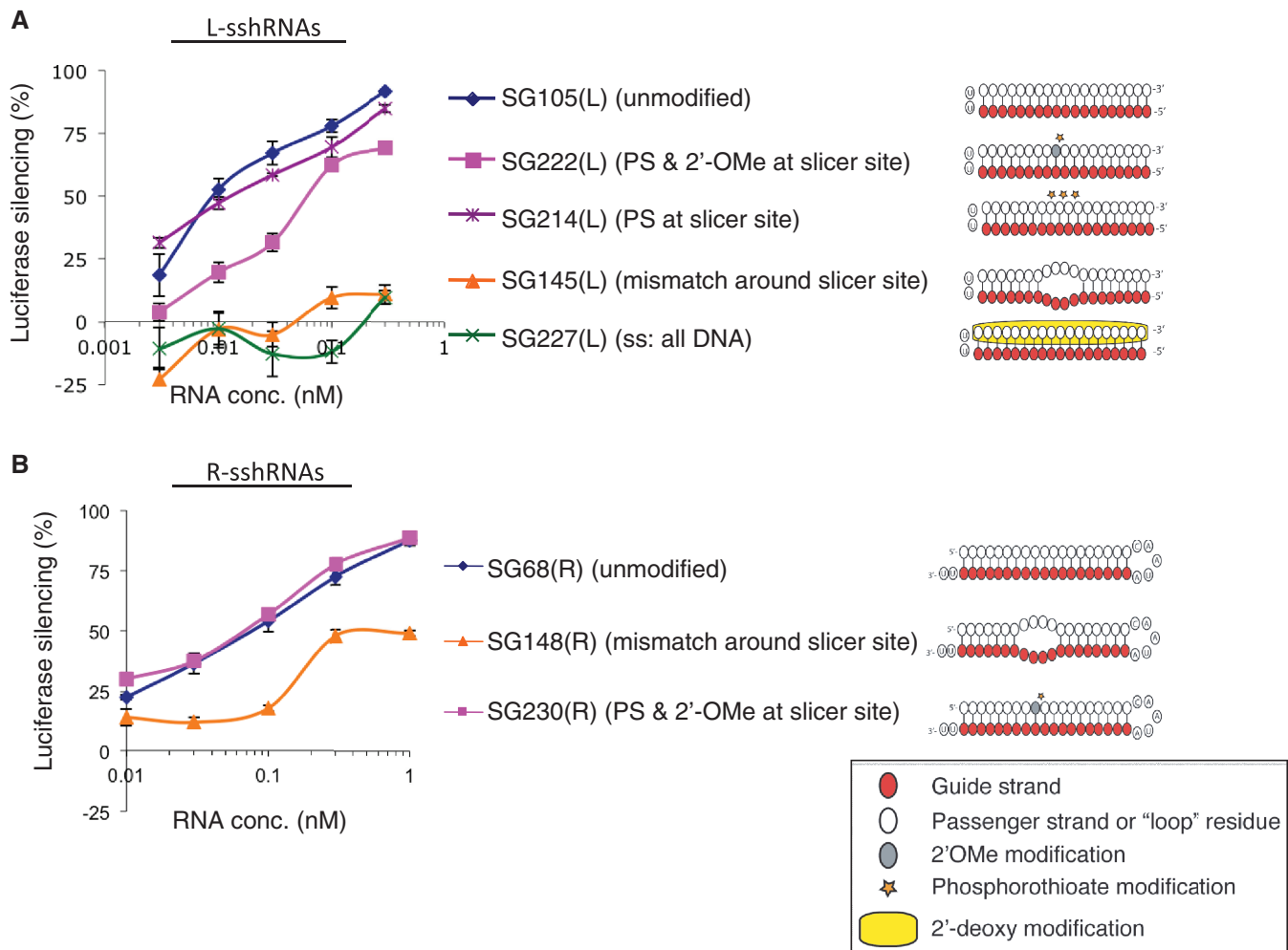


Figure 4. Comparison of L- and R-sshRNA activity with mismatches or modifications in the sense strands around the slicer site. sshRNAs against the same target were compared for their potency of suppressing the expression of the HCV IRES/fLuc reporter in 293FT cells. (A) Comparison of the dose response curves of L-sshRNAs with mismatches or modifications in the sense arm. (B) Comparison of the activity of R-sshRNAs with mismatches or modifications in the sense arm. Schematic cartoons describe the sshRNAs constructs in this figure, coded as in Figure 3.

full-length sshRNA (40 nt) and a three-quarter length molecule (30 nt), consistent with a cleavage event in the middle of the passenger arm while the loop remained intact (Figure 5A). The smaller fragment of slicing (10 nt) would not have been visualized in this experiment because it did not contain the 5' label.

For cells transfected with 5'-end labeled sh1, with its 25-bp duplex and 10-nt linker (see above), we observed two bands in the Ago2-associated fraction. The appearance of a stronger band, at a size of about 21–23 nt (Figure 5A), is consistent with Dicer processing and loss of the loop and passenger strand as expected. A faint band that co-migrates with full-length sh1 was also observed, suggesting that even hairpins with a long duplex stem can bind to Ago2 (16,43,46) (Figure 5A). This observation is consistent with our observation of silencing activity by this molecule in the Dicer knockout cell line and suggests that Dicer-independent mechanisms may accommodate both sshRNAs and conventional shRNAs like sh1 (Figure 1B). Thus, multiple pathways may be available for

processing even lshRNAs; the two strands may become detached either by Dicer processing of the stem or through loop cleavage by some other nuclease.

Cleavage of the passenger arms in L-type sshRNA-Ago2 complexes was confirmed in experiments with additional 5'-end labeled sshRNAs. Immunoprecipitation of Ago2 complexes from cells transfected with a labeled 38-nt sshRNA, SG119(L), revealed both a full-length product (38 nt) and an ~10-nt shorter product (~28 nt) associated with Ago2 (Figure 5B). For both SG224(L) and SG119(L), the major band associated with Ago2 was the 10-nt shorter band, suggesting that a large majority of the hairpins bound by Ago2 are converted into the sliced product. When the passenger-arm sequence has either mismatches [SG145(L)] or chemical modifications [SG222(L)] at the slicer cleavage site, only full-length sshRNA is associated with Ago2 (Figure 5B) and the silencing activities of both of these molecules are reduced (Figure 4B). Similar results were found for a series of sshRNAs targeting a different sequence

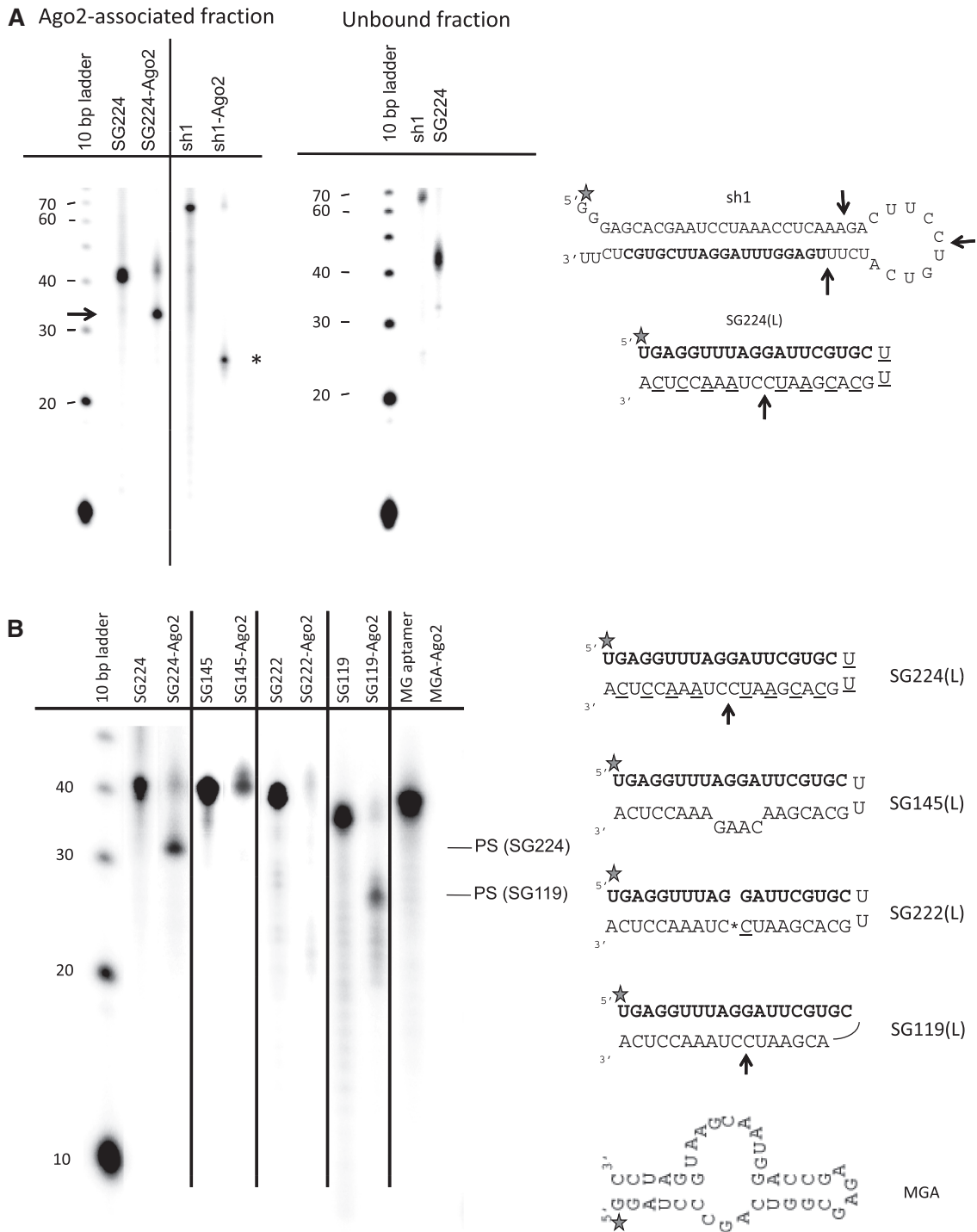


Figure 5. 5'-end-labeled L-sshRNAs show Ago2-associated bands consistent with cleavage at the passenger-strand slicer site. RNAs were 5'-end-labeled with ^{32}P (stars on sequences) and transfected into 293FT cells. Six hours later, cell lysates were prepared and incubated with anti-hAgo2 antibody for 16 h at 4°C. **(A)** Denaturing PAGE analysis of RNAs isolated from Ago2 antibody-bound complexes (left) and the fraction not bound by Ago2 (right). Full-length 5'-end-labeled shRNAs (left gel, lanes labeled SG224 and sh1) were loaded as markers alongside the RNA that co-immunoprecipitated with hAgo2 (left gel, lanes SG224-Ago2 and sh1-Ago2). An arrow points to the immunoprecipitated SG224 RNA whose length is consistent with cleavage of the passenger arm at the slicer site. An asterisk marks sh1 immunoprecipitated sh1 RNA whose length is consistent with dicer processing and/or ribonuclease cleavage in the loop. Levels of a given species cannot be compared between Ago2-associated and unbound fractions because the latter includes excess starting material and less of it was sampled in the measurement. **(B)** Comparison of Ago2-associated L-sshRNAs that are highly potent (SG224 and SS119) with sshRNAs with severely impaired activity associated with non-Watson–Crick pairing at the slicer site (SG145) and chemical modification of the passenger-arm slicer site (SG222). Malachite green aptamer (MG aptamer, MGA) was included as a negative control for hAgo2 binding. Arrows on sequences indicate the sites of cleavage in the hAgo2-associated RNAs. Bands corresponding to cleavage at the passenger-arm slicer site are labeled PS. Nucleotides that are underlined contain 2'OMe-modifications. An asterisk shows the position of phosphorothioate modification.

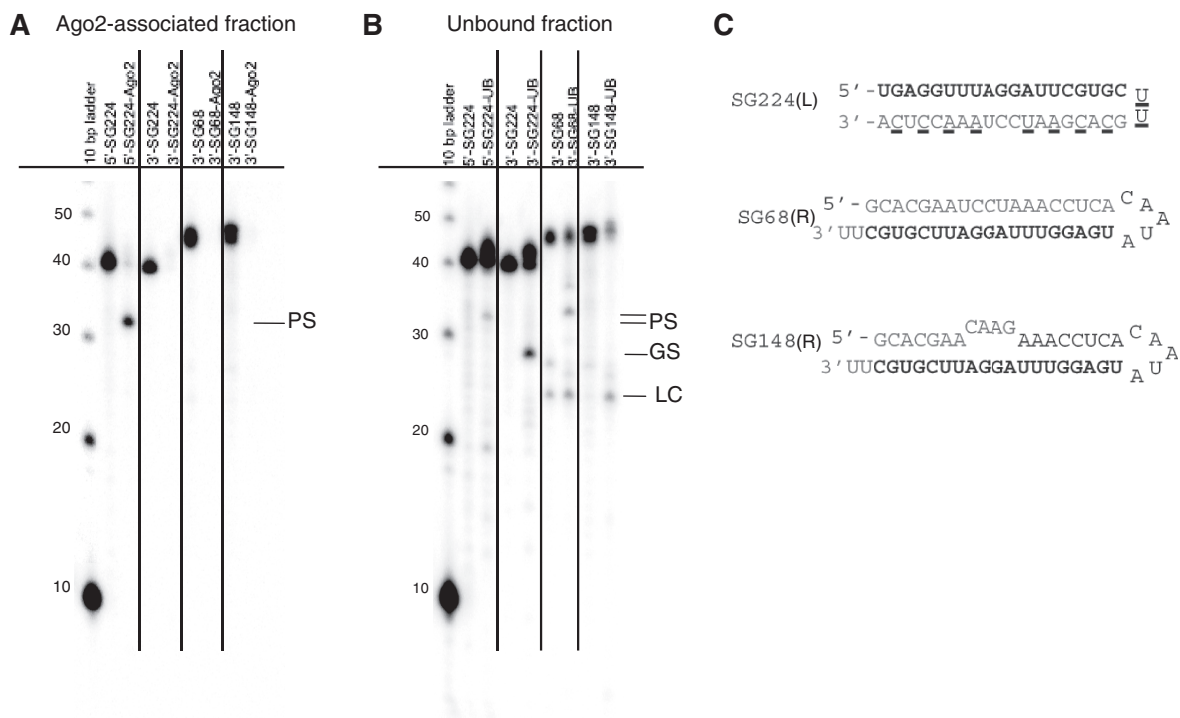


Figure 6. R-sshRNAs are not immunoprecipitated with Ago2 in either intact or sliced form. (A) Denaturing PAGE analysis of L-sshRNA SG224 and R-sshRNAs SG68 and SG148 isolated from hAgo2 antibody-bound complexes that were either 5'- or 3'-end-labeled as marked prior to transfection in 293FT cells (lanes 5'-SG224-Ago2, 3'-SG224-Ago2, 3'-SG68-Ago2, 3'-SG148-Ago2). (B) Denaturing PAGE of the supernatant fraction of L- and R-sshRNAs not immunoprecipitated by hAgo2 antibody (5'-SG224-UB, 3'-SG224-UB, 3'-SG68-UB, 3'-SG148-UB). (C) Structures of sshRNAs. Full-length 5'- and 3'-end-labeled sshRNAs (lanes in panels A and B labeled 5'-SG224, 3'-SG224, 3'-SG68 and 3'-SG148) were loaded as markers alongside the RNA that co-immunoprecipitated with Ago2. Gel bands labeled PS correspond to cleavage of sshRNA at the passenger-arm slicer site. Bands labeled GS and LC correspond to slicing of the guide sequence and cleavage of the loop, respectively.

(Supplementary Figure S4). The fact that SG145(L) binds to Ago2 reinforces the conclusion based on efficacy data (see above and Figure 4) that the mismatches in this sshRNA inactivate silencing by blocking passenger-strand slicing rather than by preventing Argonaute binding. As expected, a control RNA of similar size but different architecture (the 38-nt malachite green aptamer) showed no association with Ago2 (Figure 5B).

L-sshRNAs conform to pre-miR-451 architecture

It was recently reported that pre-miR-451, which is too short (17 bp) to be a Dicer substrate, is incorporated in its entirety into RISC and sliced in the passenger arm (10,11). After slicing, the 3'-terminus is further chewed back and a variable number of U residues are added. SG119(L) resembles pre-miR-451 in that it contains a fully paired 17-bp stem and a minimal loop consisting of the nucleotides at the 3'-end of the guide sequence. Interestingly, SG119(L) complexes with Ago2 show the same distribution of lengths as seen with miR-451, suggesting that this molecule may be processed in a similar way (Figure 5B). However, SG224(L), with a 19-bp stem, shows only a single sliced product of ~30 nt bound to Ago2, suggesting that the pattern of processing seen with miR-451 may require a stem shorter than 19 bp (Figure 5A and B). Taken together, these results indicate that L-sshRNAs, like pre-miR-451, utilize a natural,

Dicer-independent RISC-loading pathway followed by Ago2-mediated activation.

Slicing can occur in the 5' arm of sshRNAs

To examine whether R-sshRNAs were also loaded into Ago2 and processed at the slicer site of their passenger strands, Ago2 pull-down experiments were performed with 3'-end-labeled sshRNAs. Neither full-length nor processed R-sshRNAs were observed in immunoprecipitated Ago2 complexes (Figure 6A) although the limit of detection of these species was less than for L-sshRNAs because the 3'-ends are less efficiently labeled. However, in the unbound (supernatant) fraction, an RNA fragment of the length predicted for cleavage at the slicer site of the passenger arm (without loop cleavage) of the R-sshRNA SG68(R) was detected (Figure 6B, 3'-SG68-UB). Passenger-arm slicing of R-sshRNAs cleaves off the 5'-proximal 10 nt of the molecule (including the 5'-phosphate that presumably anchors the sshRNA into the MID domain), which might account for the lack of stable association with Ago. As with the L-sshRNAs, when an R-sshRNA had slicer-site mismatches [SG148(R)], no passenger-strand slicing was evident, either in the bound or unbound fractions. However, in the unbound fraction of both SG68(R) and SG148(R), there was a fragment of about 23 nt consistent with cleavage in the loop (Figure 6B),

again emphasizing the distinct pathways of action of R- and L-sshRNAs. Both of these sshRNAs have unmodified 5-nt linkers (CAAUA) containing two pyrimidine-adenosine sequences (CA and UA) that could be susceptible to cleavage by a ribonuclease. The passenger strand could be subsequently removed by unwinding by a helicase (53) or degradation by C3PO (19,47). Indeed, the activity of an R-sshRNA with four mismatches around the slicing site [SG148(R)] was only partially reduced (Figure 4B), consistent with duplex separation for this R-sshRNA occurring via loop cleavage instead of passenger-strand slicing.

Strand selection for entry into RISC

A nominally L-type shRNA such as SG224(L) could act as an R-type if the 3' arm of the hairpin (the sense arm) is recognized as the guide strand and the 5' arm (antisense) is treated as the passenger strand and sliced. Labeling of SG224(L) at its 3'-end allows visualization of any slicing of its 5' (antisense) arm. Indeed, upon 3'-end labeling we observed a ~30-nt fragment consistent with cleavage in the 5' (antisense) arm, but only in the unbound fraction (Figure 6B, 3'-SG224-UB). Thus, as with other R-type sshRNAs, this processing product does not stably associate with Ago2, and it appears in much lower yield than when slicing occurs when the 5' arm of the hairpin is recognized as the guide strand (Figure 6A, 5'-SG224-Ago2). These data suggest that L-sshRNAs can be loaded into RISC in two different orientations and that slicing can occur on either arm of the hairpin, but only slicing in the 3' arm and loss of the resulting smaller fragment leaves a guide strand with a 5'-phosphate and a seed sequence that is unpaired and available for hybridizing with a target.

The lack of a 3'-labeled 10-nt fragment of SG224(L) in either the Ago2-bound or unbound fractions despite the high proportion of sliced product in the Ago2-associated fraction (Figure 6A and B) suggests that this fragment is rapidly degraded, either by C3PO or some other cellular nuclease.

'Pre-sliced' sshRNAs are functionally inactive and are not immunoprecipitated by Ago2 antibodies

Having detected sliced L-sshRNAs complexed to Ago2, we asked whether such fragments themselves would be active in either Ago2 binding or silencing. To address this question, we synthesized a truncated sshRNA with the same sequence and modification patterns as the expected product of cleavage of SG224(L) at the passenger-strand slicer site [SG244(L)]. The efficacy of target knockdown was compared after transfection of the 'pre-sliced' SG244(L), the full-length, unprocessed SG224(L), or a full-length scrambled control (SG221) into 293FT cells. Although the 5' single-stranded region of SG244(L) may be susceptible to degradation by a nuclease, any such activity would remove the 5'-³²P-label; hence, this experiment addresses the activity of intact SG244(L). We observed that SG244(L) showed neither silencing activity (Figure 7A) nor stable binding

to Ago2 based on immunoprecipitation with anti-hAgo2 antibodies (Figure 7B). These results suggest that, although Ago2 can slice SG224(L) and remain bound to the 30-nt product of that cleavage reaction, it will not bind this product if it is free in the cytosol, evidently because duplex structure at the 5'-end is necessary for efficient RISC-loading. Since there is no binding, the molecule is inactive.

Both L- and R-sshRNAs can be loaded into Ago1-containing complexes and sliced

To assess a possible role for Ago1 in silencing by sshRNAs, pull-down experiments were also performed with antibodies that have been shown to be specific for hAgo1 without cross-reactivity to hAgo2 (68). For the small-linker L-sshRNA SG224(L), both full-length RNA and a 30 nt RNA consistent with cleavage at the normal passenger-arm slicer site (10 nt from the 3'-end of the passenger arm) were detected by denaturing PAGE analysis of the Ago1-bound fraction (Figure 8A), although the extent of cleavage was not as complete as with Ago2 complexes (Figures 5 and 6). These results are consistent with both Ago1 and Ago2 being capable of processing L-sshRNAs in a Dicer-cleavage independent mechanism, and in accordance with a previous report of miRNA and siRNA slicing by Ago1 in a cell-free system (42). In another study involving cultured cells, efficient passenger strand removal was not observed with Ago1 siRNA complexes (49), which the authors interpreted as indicative of Ago1 not slicing the passenger strand. However, because pre-sliced sshRNAs did not associate with Ago2 (Figure 7), the association of a sliced sshRNA with Ago1 suggests that Ago1 was indeed responsible for slicing the molecule to which it was bound, rather than binding to a molecule that had been already sliced by Ago2.

When SG224(L) was 3'-end-labeled, a fragment consistent with the 30 nt product of guide strand cleavage was found in the unbound but not the bound fraction, suggesting that it does not stably associate with either Ago1 (Figure 8A and B) or Ago2 (Figure 6). Thus, only 'correct' (passenger arm) slicing of L-sshRNAs leads to stable binding to Ago1 and Ago2, possibly because slicing of the 'wrong' (guide) strand allows the large cleavage fragment to dissociate from the smaller fragment that is anchored to the MID domain through its 5'-phosphate.

For the R-types SG68(R), SG148(R) and SG150(R), a weak band corresponding to full-length sshRNA was associated with Ago1 (Figure 8C). Of these R-sshRNAs, the fully matched SG68(R) and SG150(R) showed evidence of passenger-strand slicing only in the unbound fraction, with no Ago1 complex seen (Figure 8C and D). SG148(R), which has mismatches at those positions, showed no slicing in either the Ago1-associated or unbound fractions, as expected. Fragments consistent with cleavage at the 5-nt unmodified loops of SG68(R) and SG148(R) were observed in both the Ago1-associated and unbound fractions, whereas the unmodified dinucleotide UU linker of SG150(R) was not cleaved (Figure 8C and D). Passenger-strand slicing of R-sshRNAs in the

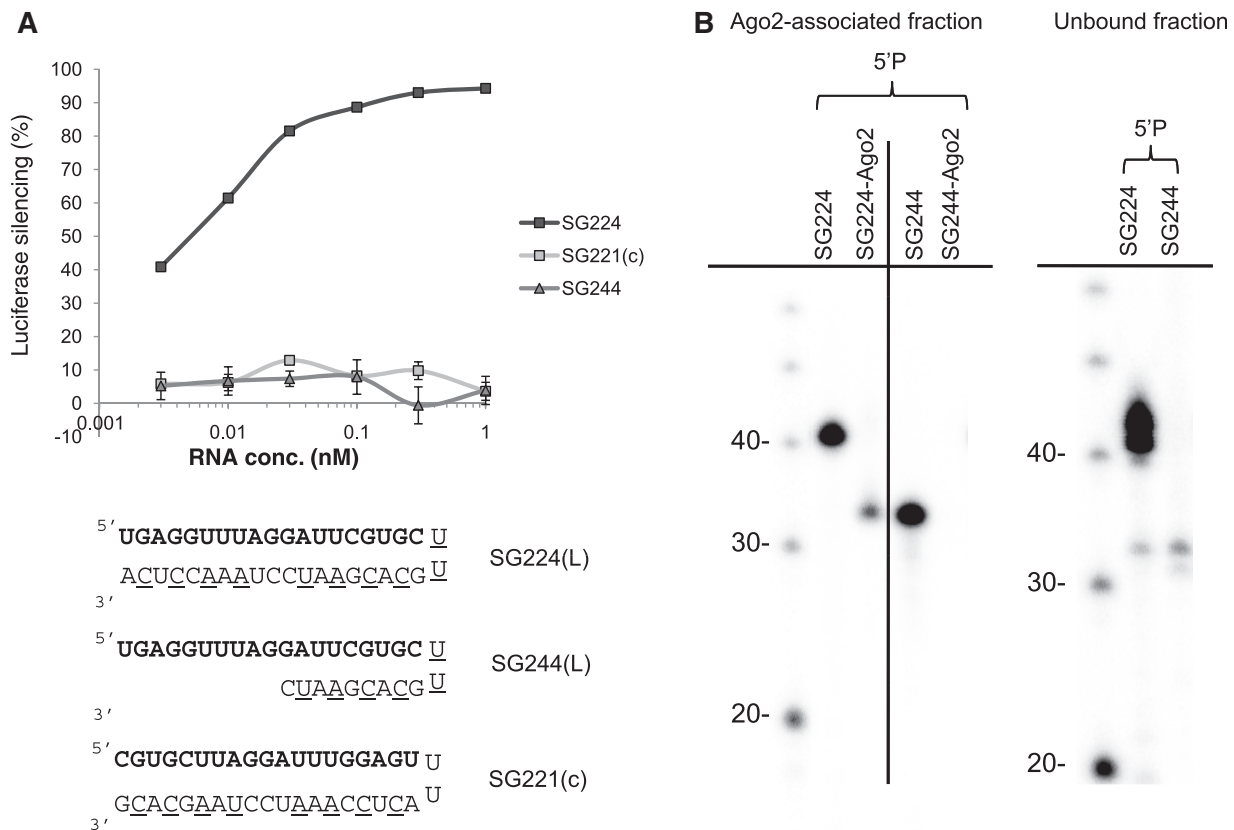


Figure 7. Synthetic 'pre-sliced' sshRNA does not knock down target expression and is not immunoprecipitated by Ago2, indicating that a fully base-paired stem is required for RISC-loading. (A) Comparison of activity of L-sshRNA SG224 with SG244, a synthetic analog of the product of the cleavage of the sense arm at the slicer site. SG221(c) is a scrambled control sshRNA. (B) Denaturing gel analysis of Ago2-associated RNAs for 5'-end-labeled SG224 (left) and SG244 (right).

absence of loop cleavage would be similar to 'wrong' strand cleavage of L-sshRNAs, which appears to lead to dissociation of the large fragment from the Ago complex (see above) and loss of activity, thus explaining the finding of ~30-nt fragments of SG68(R) and SG150(R) only in the unbound fraction. If the 5-nt linker is cleaved before slicing, the resulting free 3' arm can load into Ago as a guide strand, with its 'new' 5'-phosphate anchoring in the MID-binding pocket. The separated passenger strand can be sliced and the 10-nt fragments will be dissociated and/or degraded as with any siRNA. These results further support the hypothesis that the main pathway of R-sshRNAs function is through loop cleavage rather than slicing alone.

The presence of a target does not influence the choice of which arm of an sshRNA is selected to be the guide strand in active RISC

An shRNA is defined as L or R only with reference to a target sequence. The same hairpin sequence is L if its 5' half is antisense to its target, and R if its 3' half is antisense. Thus, an R-type sshRNA could theoretically be sliced in its antisense arm as if it were an L-sshRNA. For sshRNAs as well as siRNAs, the choice of which strand is retained to become the guide strand could be

determined solely by the structure and sequence of the sshRNA or, alternatively, the presence of a target complementary to one arm or the other could play a role. The latter possibility could account for why, for example, effective R-sshRNAs select the 3' arm of the hairpin as the guide strand despite the additional need for loop cleavage to define the 5'-end of the guide sequence.

To determine whether the presence of a target influences the choice of which part of the hairpin is retained in RISC, we made a pair of reporter constructs in which a target sequence complementary to either the sense or antisense segments of a series of sshRNAs was inserted into the 3'-UTR of rLuc in a psiCHECK-based (Promega, Madison, WI) dual luciferase reporter plasmid (psiCHECK-2-pIRES, Supplementary Figure S6). The resulting 'forward' plasmid tests the efficiency of RNAi using the antisense sequence as the guide and the sense sequence as the target, and the 'reverse' plasmid (with the antisense sequence as the target) tests for use of the sense sequence of the sshRNA as the guide. The parent plasmid with no insert was used as a control. L- and R-sshRNAs were synthesized with both 5- and 2-nt linkers and co-transfected into 293FT cells along with one or the other of the reporter plasmids (Supplementary Figure S6). In all cases (including both

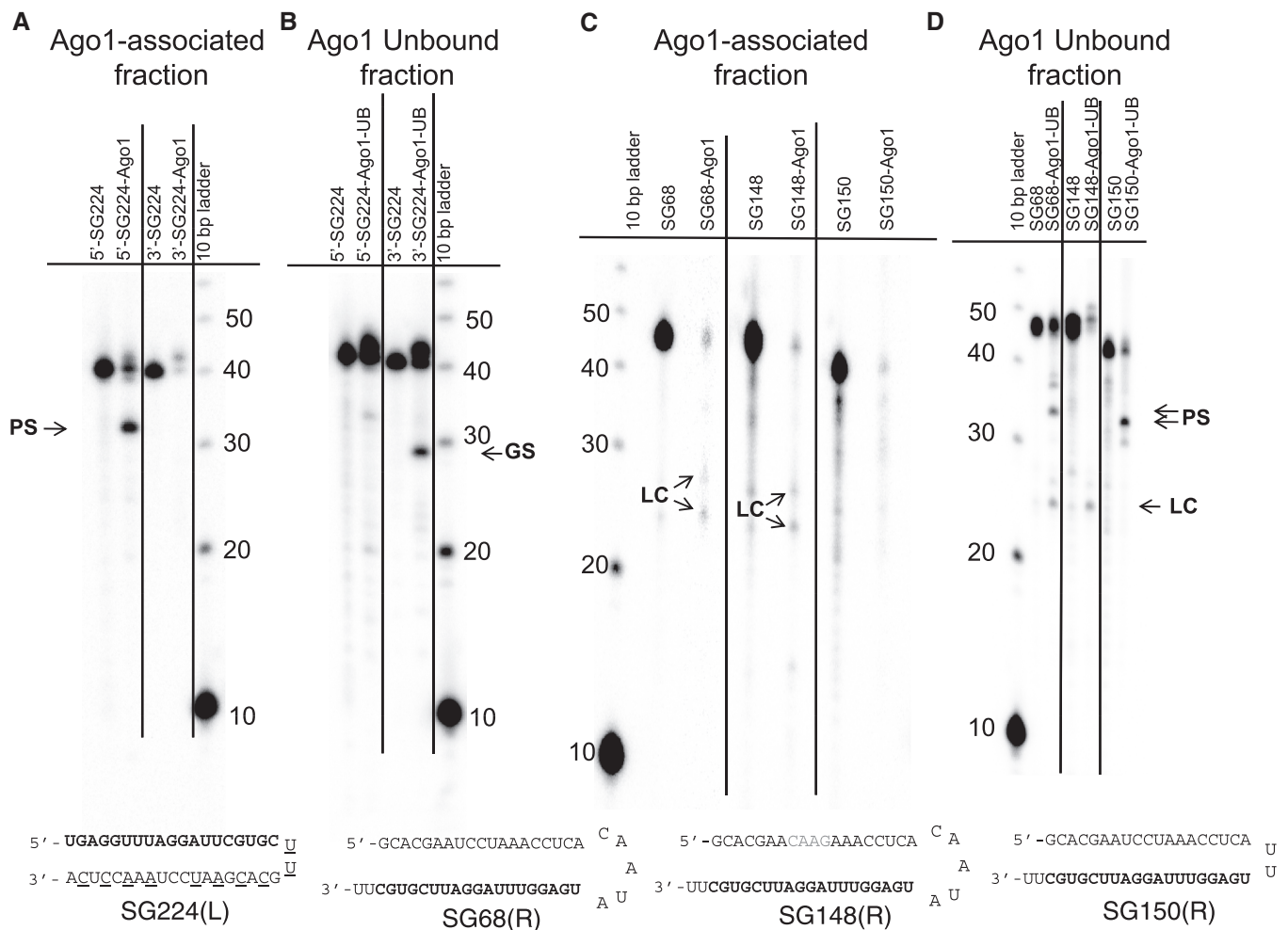


Figure 8. End-labeled RNAs detected by co-immunoprecipitation with hAgo1 antibodies. (A) Denaturing PAGE analysis of SG224 L-shsRNAs isolated from Ago1 antibody-bound complexes that were either 5'- or 3'-end-labeled as marked prior to transfection in 293FT cells (lanes 5'-SG224-Ago1 and 3'-SG224-Ago1, respectively) (B) Denaturing PAGE of the supernatant fraction of L-shsRNAs not immunoprecipitated by hAgo1 antibody (5'-SG224-Ago-UB and 3'-SG224-Ago1-UB, respectively). Full-length 5' and 3'-end-labeled shRNAs [lanes in (A) and (B) labeled 5'-SG224 and 3'-SG224] were loaded as markers alongside the RNA that co-immunoprecipitated with hAgo1. An arrow points to the immunoprecipitated SG224 RNA whose length is consistent with cleavage of the passenger arm at the slicer site. (C) Comparison of 3'-end-labeled R-shsRNAs isolated from Ago1 antibody-bound complexes that are active (lanes SG68-Ago1 and SG150-Ago1) with an R-shsRNA containing mismatches at the slicer site with reduced activity (SG148-Ago1) as well as the RNA fraction remaining unbound to hAgo1 antibodies (D). PS (passenger strand sliced), GS (guide strand sliced), LC (loop cleaved).

R- and L-orientations), only the expression of the forward (sense) target was inhibited; in no case did the expression of the reverse (antisense) target show any inhibition by the use of the 'wrong' part of the hairpin as guide. This same result was observed for three separate targets (Supplementary Figure S6 and data not shown). Moreover, no effect of the presence of either target plasmid was seen in Ago2 immunoprecipitation experiments with labeled SG224(L) (Supplementary Figure S7). For the antisense target of the series of sshRNAs targeting site 74, rLuc expression showed some inhibition at 3 nM sshRNA, suggesting the existence of either targeting by the 'wrong' strand or nonspecific effects at that concentration. In our experience, most sshRNAs as well as siRNAs begin to show some nonspecific target inhibition in these assays at concentrations ranging from 3 to 10 nM. The IC₅₀s of all active sshRNAs were well below 3 nM, so the reporter gene suppression seen for both L- and

R-shsRNAs in Figures 1, 2, 4 and Supplementary Figure S6 are antisense strand-directed, specific, on-target effects. The target-swapping results suggest that, for both the L- and R-forms of these sshRNAs, the sense arms were not efficiently retained in active RISC or, to the extent that they were retained, they were ineffective at binding to or cleaving a complementary target.

The fact that the presence of the target does not affect which sequence of an sshRNA is retained in active RISC indicates that the sequence and/or structure of the hairpins are the determining factor(s). In the case of siRNAs, asymmetry in helix stability is often a key determinant of strand selection and potency (21,63). To see if this asymmetry also holds for effective sshRNAs, the internal stability profiles of L- and R-shsRNAs were compared. However, no correlation was seen between efficacy and helix stability at the 5'-end of the antisense sequence (Supplementary Figure S8), suggesting that the

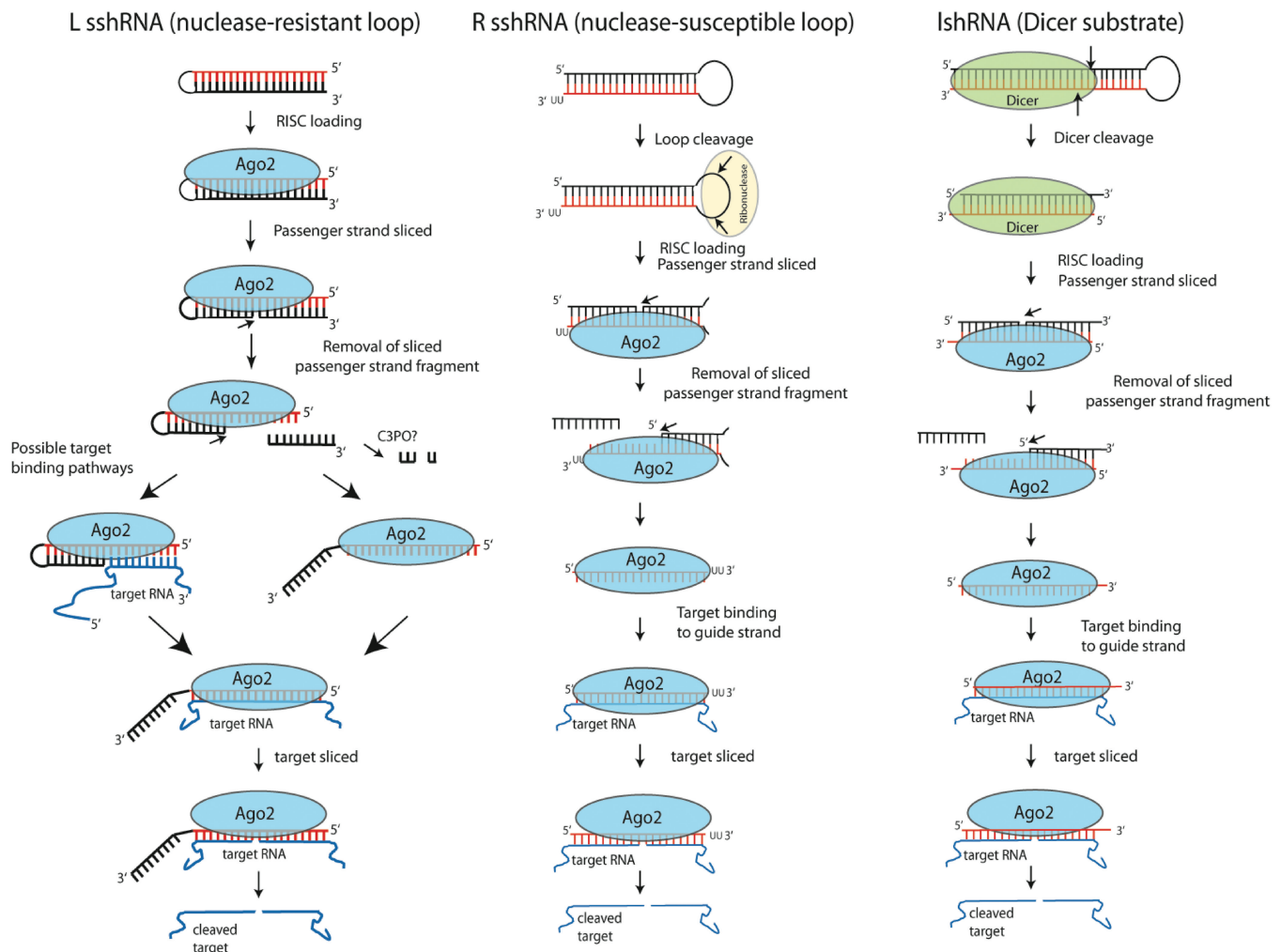


Figure 9. Proposed mechanisms of Dicer-independent processing by hAgo2 of L-sshRNAs with short, nuclease resistant loops (left column) and R-sshRNAs with longer, nuclease susceptible loops (middle column) alongside canonical Dicer-substrate IshRNAs (right column). L-sshRNAs are loaded directly into RISC without prior cleavage of the loop. The guide arm becomes available for target pairing after passenger-arm slicing by Ago2 (or Ago1, not shown). For optimal activity, the loops of R-sshRNAs need to be cleaved by an unspecified cellular endonuclease to facilitate removal of the passenger strand of the duplex. IshRNAs are first cleaved by Dicer prior to RISC activation. Red lines are guide sequence; black lines, passenger sequence; and blue lines, target RNA. Not drawn to scale.

presence of the loop has an important influence on strand selection and potency. If that loop is resistant to cleavage, it provides a natural strand bias toward recognition as the L-form, in which case there is a terminal phosphate group at the 5'-end of the antisense sequence. This natural strand bias suggests that L-sshRNAs may be less prone to off-target effects resulting from selection of the sense sequence as the guide compared to siRNAs. For such cleavage-resistant loops, the L-forms are indeed more potent than the corresponding R-forms. Where the loop is easily cleaved, R-sshRNAs may be as potent as their L-counterparts (Figure 2D).

Model for the differing mechanisms of action of L- and R-sshRNAs

The results presented above suggest a model for the mechanisms of action of L- and R-sshRNAs, shown in Figure 9. L-sshRNAs are loaded directly into RISC

because the 5'-phosphate on the guide arm is available for docking in the MID-domain binding pocket of Ago2 as observed in eubacterial (32–34), archaeal (31) and eukaryotic (69) crystal structures of the MID domain and the entire hAgo2 (35). Efficient loading requires duplex structure at the 5'-end; hence pre-sliced L-sshRNAs are not loaded and therefore are functionally inactive. Once loaded, the passenger arm of the L-sshRNA is sliced and the resulting small 3' fragment is lost from the complex, probably through degradation by C3PO as has been observed for siRNAs (19,47). The seed sequence is now single-stranded and readily available to bind to a target RNA, after which the target could displace the remaining part of the passenger arm by branch migration to allow maximal pairing between the guide sequence and the target. The displaced 3'-end of the sliced sshRNA, like the 3' overhangs of siRNAs, is now available for binding to the PAZ domain of Ago. Since only L-sshRNAs that

have been sliced in the passenger arm form stable complexes with Argonaute proteins, L-sshRNAs have a built-in asymmetry sensor (a nuclease-resistant loop) that allows for correct selection of which arm becomes the guide sequence, as opposed to the thermodynamic asymmetry sensor used by siRNAs. In this way, potential off-target effects resulting from sense sequence targeting may be avoided. This on-target bias is enhanced for L-sshRNAs with small or chemically modified linkers that are resistant to nuclease cleavage, because that design precludes formation of a 5'-phosphate at the end of the sense sequence and thus disallows use of the 'wrong' arm as the guide sequence. An additional prediction of this scheme is that a target sequence that corresponds to a potent L-sshRNA may not always make for a potent siRNA because it is not required to have the same thermodynamic asymmetry, but any potent siRNA should correspond to a potent L-sshRNA.

For an R-sshRNA to be potent, its loop must be cleavable, and that cleavage must occur prior to productive formation of active RISC. Upon loop cleavage, a 5'-phosphate is either produced by the cleavage reaction or (if cleavage produces a 3'-OH) subsequently added by an endogenous kinase at or near the first nucleotide of the guide strand. This 5'-phosphate promotes stable binding and accurate positioning of the guide strand in a complex with the MID domain of either Ago1 or Ago2 (31–35). The passenger strand may be sliced to facilitate its removal and leave the guide strand available for pairing with the target. If passenger-strand slicing is blocked by chemical modification or impaired by mismatches at the slicer site, displacement of the passenger strand, presumably by a helicase activity, may still occur. However, if passenger-strand slicing occurs without loop cleavage of R-sshRNAs, there would be no phosphate at the 5'-end of the guide sequence. A steric clash would presumably interfere with guide sequence docking into the MID domain of Ago2 or Ago1, or it might be inaccurately positioned in RISC. Such defective positioning could account for the less accurate target cleavage sites mapped by 5'-RACE for R-sshRNAs with chemically-modified loops compared with similar L-sshRNAs. Another factor that might explain the reduced activity of R-sshRNA with small or modified loops is that, unlike L-sshRNAs, the seed region of the guide strand of R-sshRNAs may remain double-stranded even after slicing, leaving it less available for target binding. Finally, whereas L-sshRNAs, upon slicing of the passenger arms and opening of the duplex, have a 3' tail for anchoring into the PAZ domain of Ago, the guide strand of R-type sshRNAs (sliced or unsliced) has no built-in 3'-extension. This difference probably accounts for the need to include a 3'-dinucleotide overhang in the design of R- (but not L-) sshRNAs for optimal silencing activity.

Although the endonuclease responsible for loop cleavage in our studies is unknown, the presence of pyrimidine-A dinucleotides in the loops of the active R-sshRNAs suggests that it might be related to RNase A. Another possible enzyme is MCP1P1, which suppresses miRNA biosynthesis via cleavage of the terminal loops of pre-miRNAs (65). UU linkers are resistant to the

endonuclease, as L-sshRNAs with this loop structure stably associated with Ago1 and Ago2 are sliced but not cleaved at the loop.

A key mechanistic issue for RNAi is how one of the two strands (if siRNA) or arms (if shRNA) is selected to be the passenger strand and sliced. Our results suggest a possible mechanism in the case of sshRNAs. If the linker is short or chemically-modified to be endonuclease resistant, it remains intact and the docking of the single 5'-phosphate into the MID pocket determines the orientation of binding. Most of the time, that orientation results in slicing of the 3' arm (L-type mechanism). However, we see some slicing of the 5' arm (Figure 6B), suggesting two possibilities: (i) a conformational change sometimes allows that arm to juxtapose with the active site of Ago2, resulting in separation of the docked 5'-end from the main part of the molecule, which then dissociates from Ago2; or (ii) the hairpin can sometimes bind with the loop (instead of the 5'-end) proximal to the MID pocket. In that case, the small fragment dissociates and the new 5'-end of the large fragment is poorly positioned to target any mRNA. For both L- and R-shRNAs, if the loop is large enough to allow cleavage prior to Ago2 binding, the sshRNA is converted to an siRNA and choice of passenger strand is determined accordingly, apparently dictated by thermodynamic asymmetry.

CONCLUSION

L-sshRNAs do not require loop cleavage but do require slicing of the passenger arm to achieve maximal potency in silencing. In contrast, R-sshRNAs do require loop cleavage for maximal potency. This explains how R-sshRNAs can be potent RNAi effectors even though they do not have a 5'-phosphate at the end of their guide arm. R-sshRNAs do not require passenger-strand slicing but are more effective when it can occur. Slicing of the passenger strand may be mediated by either Ago2 or Ago1, and Ago2 appears to require at least one helical turn of duplex (≥ 11 bp) to bind. The results are consistent with a model in which effective L-sshRNAs remain in active RISC and induce target cleavage as three-quarter-length single strands, while effective R-sshRNAs are cleaved at the loop, facilitating removal of the entire passenger strand and subsequent targeting by the guide strand. L-sshRNAs may be less prone to off-target silencing by the sense strand than other types of RNAi agents because only molecules that are sliced in the passenger arm are retained in RISC.

SUPPLEMENTARY DATA

Supplementary Data are available at NAR Online: Supplementary Table 1, Supplementary Figures 1–8, and Supplementary Materials and Methods.

ACKNOWLEDGEMENTS

We thank Dr Thomas Tuschl for helpful advice on Argonaute immunoprecipitation, Dr John Rossi for

useful discussions and Dr Sumedha Jayasena for comments on the manuscript.

FUNDING

National Institutes of Health (NIH) [R44AI056611, R44AI074256 and R43AI074214 to B.H.J., and RO1GM80783 and UCSF DERC DK063720 to M.T.M.]. Funding for open access charge: NIH [R44AI056611, R44AI074256 and R43AI074214 to B.H.J.].


Conflict of interest statement. None declared.

REFERENCES

- Filipowicz,W. (2005) RNAi: the nuts and bolts of the RISC machine. *Cell*, **122**, 17–20.
- Siomi,H. and Siomi,M.C. (2009) On the road to reading the RNA-interference code. *Nature*, **457**, 396–404.
- Ender,C. and Meister,G. (2010) Argonaute proteins at a glance. *J. Cell Sci.*, **123**, 1819–1823.
- Hammond,S.M., Bernstein,E., Beach,D. and Hannon,G.J. (2000) An RNA-directed nuclease mediates post-transcriptional gene silencing in *Drosophila* cells. *Nature*, **404**, 293–296.
- Zamore,P.D., Tuschl,T., Sharp,P.A. and Bartel,D.P. (2000) RNAi: double-stranded RNA directs the ATP-dependent cleavage of mRNA at 21 to 23 nucleotide intervals. *Cell*, **101**, 25–33.
- Bernstein,E., Caudy,A.A., Hammond,S.M. and Hannon,G.J. (2001) Role for a bidentate ribonuclease in the initiation step of RNA interference. *Nature*, **409**, 363–366.
- Elbashir,S.M., Lendeckel,W. and Tuschl,T. (2001) RNA interference is mediated by 21- and 22-nucleotide RNAs. *Genes Dev.*, **15**, 188–200.
- Ge,Q., Ilves,H., Dallas,A., Kumar,P., Shorestein,J., Kazakov,S.A. and Johnston,B.H. (2010) Minimal-length short hairpin RNAs: the relationship of structure and RNAi activity. *RNA*, **16**, 106–117.
- Siolas,D., Lerner,C., Burchard,J., Ge,W., Linsley,P.S., Paddison,P.J., Hannon,G.J. and Cleary,M.A. (2005) Synthetic shRNAs as potent RNAi triggers. *Nat. Biotechnol.*, **23**, 227–231.
- Cifuentes,D., Xue,H., Taylor,D.W., Patnode,H., Mishima,Y., Cheloufi,S., Ma,E., Mane,S., Hannon,G.J., Lawson,N.D. *et al.* (2010) A novel miRNA processing pathway independent of Dicer requires Argonaute2 catalytic activity. *Science*, **328**, 1694–1698.
- Cheloufi,S., Dos Santos,C.O., Chong,M.M. and Hannon,G.J. (2010) A dicer-independent miRNA biogenesis pathway that requires Ago catalysis. *Nature*, **465**, 584–589.
- Chendrimada,T.P., Gregory,R.I., Kumaraswamy,E., Norman,J., Cooch,N., Nishikura,K. and Shiekhattar,R. (2005) TRBP recruits the Dicer complex to Ago2 for microRNA processing and gene silencing. *Nature*, **436**, 740–744.
- Gregory,R.I., Chendrimada,T.P., Cooch,N. and Shiekhattar,R. (2005) Human RISC couples microRNA biogenesis and posttranscriptional gene silencing. *Cell*, **123**, 631–640.
- MacRae,I.J., Ma,E., Zhou,M., Robinson,C.V. and Doudna,J.A. (2008) In vitro reconstitution of the human RISC-loading complex. *Proc. Natl Acad. Sci. USA*, **105**, 512–517.
- Maniataki,E. and Mourelatos,Z. (2005) A human, ATP-independent, RISC assembly machine fueled by pre-miRNA. *Genes Dev.*, **19**, 2979–2990.
- Tan,G.S., Garchow,B.G., Liu,X., Yeung,J., Morris,J.P. IV, Cuellar,T.L., McManus,M.T. and Kiriakidou,M. (2009) Expanded RNA-binding activities of mammalian Argonaute 2. *Nucleic Acids Res.*, **37**, 7533–7545.
- Kanellopoulou,C., Muljo,S.A., Kung,A.L., Ganesan,S., Drapkin,R., Jenuwein,T., Livingston,D.M. and Rajewsky,K. (2005) Dicer-deficient mouse embryonic stem cells are defective in differentiation and centromeric silencing. *Genes Dev.*, **19**, 489–501.
- Murchison,E.P., Partridge,J.F., Tam,O.H., Cheloufi,S. and Hannon,G.J. (2005) Characterization of Dicer-deficient murine embryonic stem cells. *Proc. Natl Acad. Sci. USA*, **102**, 12135–12140.
- Ye,X., Huang,N., Liu,Y., Paroo,Z., Huerta,C., Li,P., Chen,S., Liu,Q. and Zhang,H. (2011) Structure of C3PO and mechanism of human RISC activation. *Nat. Struct. Mol. Biol.*, **18**, 650–657.
- Schwarz,D.S., Tomari,Y. and Zamore,P.D. (2004) The RNA-induced silencing complex is a Mg²⁺-dependent endonuclease. *Curr. Biol.*, **14**, 787–791.
- Khvorova,A., Reynolds,A. and Jayasena,S.D. (2003) Functional siRNAs and miRNAs exhibit strand bias. *Cell*, **115**, 209–216.
- Noland,C.L., Ma,E. and Doudna,J.A. (2011) siRNA repositioning for guide strand selection by human Dicer complexes. *Mol. Cell*, **43**, 110–121.
- Hutvagner,G. and Simard,M.J. (2008) Argonaute proteins: key players in RNA silencing. *Nat. Rev. Mol. Cell Biol.*, **9**, 22–32.
- Song,J.J., Smith,S.K., Hannon,G.J. and Joshua-Tor,L. (2004) Crystal structure of Argonaute and its implications for RISC slicer activity. *Science*, **305**, 1434–1437.
- Parker,J.S., Roe,S.M. and Barford,D. (2004) Crystal structure of a PIWI protein suggests mechanisms for siRNA recognition and slicer activity. *Embo. J.*, **23**, 4727–4737.
- Yuan,Y.R., Pei,Y., Ma,J.B., Kuryavyi,V., Zhadina,M., Meister,G., Chen,H.Y., Dauter,Z., Tuschl,T. and Patel,D.J. (2005) Crystal structure of *A. aeolicus* argonaute, a site-specific DNA-guided endoribonuclease, provides insights into RISC-mediated mRNA cleavage. *Mol. Cell*, **19**, 405–419.
- Liu,J., Carmell,M.A., Rivas,F.V., Marsden,C.G., Thomson,J.M., Song,J.J., Hammond,S.M., Joshua-Tor,L. and Hannon,G.J. (2004) Argonaute2 is the catalytic engine of mammalian RNAi. *Science*, **305**, 1437–1441.
- Meister,G., Landthaler,M., Patkaniowska,A., Dorsett,Y., Teng,G. and Tuschl,T. (2004) Human Argonaute2 mediates RNA cleavage targeted by miRNAs and siRNAs. *Mol. Cell*, **15**, 185–197.
- Rand,T.A., Ginalski,K., Grishin,N.V. and Wang,X. (2004) Biochemical identification of Argonaute 2 as the sole protein required for RNA-induced silencing complex activity. *Proc. Natl Acad. Sci. USA*, **101**, 14385–14389.
- Rivas,F.V., Tolia,N.H., Song,J.J., Aragon,J.P., Liu,J., Hannon,G.J. and Joshua-Tor,L. (2005) Purified Argonaute2 and an siRNA form recombinant human RISC. *Nat. Struct. Mol. Biol.*, **12**, 340–349.
- Ma,J.B., Yuan,Y.R., Meister,G., Pei,Y., Tuschl,T. and Patel,D.J. (2005) Structural basis for 5'-end-specific recognition of guide RNA by the *A. fulgidus* Piwi protein. *Nature*, **434**, 666–670.
- Wang,Y., Juranek,S., Li,H., Sheng,G., Tuschl,T. and Patel,D.J. (2008) Structure of an argonaute silencing complex with a seed-containing guide DNA and target RNA duplex. *Nature*, **456**, 921–926.
- Wang,Y., Juranek,S., Li,H., Sheng,G., Wardle,G.S., Tuschl,T. and Patel,D.J. (2009) Nucleation, propagation and cleavage of target RNAs in Ago silencing complexes. *Nature*, **461**, 754–761.
- Wang,Y., Sheng,G., Juranek,S., Tuschl,T. and Patel,D.J. (2008) Structure of the guide-strand-containing argonaute silencing complex. *Nature*, **456**, 209–213.
- Schirle,N.T. and MacRae,I.J. (2012) The crystal structure of human Argonaute2. *Science*, **336**, 1037–1040.
- Lingel,A., Simon,B., Izaurralde,E. and Sattler,M. (2004) Nucleic acid 3'-end recognition by the Argonaute2 PAZ domain. *Nat. Struct. Mol. Biol.*, **11**, 576–577.
- Ma,J.B., Ye,K. and Patel,D.J. (2004) Structural basis for overhang-specific small interfering RNA recognition by the PAZ domain. *Nature*, **429**, 318–322.
- Filipowicz,W., Bhattacharyya,S.N. and Sonenberg,N. (2008) Mechanisms of post-transcriptional regulation by microRNAs: are the answers in sight? *Nat. Rev. Genet.*, **9**, 102–114.
- Jackson,R.J. and Standart,N. (2007) How do microRNAs regulate gene expression? *Sci. STKE*, **2007**, re1.
- Tomari,Y., Du,T. and Zamore,P.D. (2007) Sorting of *Drosophila* small silencing RNAs. *Cell*, **130**, 299–308.
- Gu,S., Jin,L., Zhang,F., Huang,Y., Grimm,D., Rossi,J.J. and Kay,M.A. (2011) Thermodynamic stability of small hairpin RNAs highly influences the loading process of different mammalian Argonautes. *Proc. Natl Acad. Sci. USA*, **108**, 9208–9213.
- Wang,B., Li,S., Qi,H.H., Chowdhury,D., Shi,Y. and Novina,C.D. (2009) Distinct passenger strand and mRNA cleavage activities of human Argonaute proteins. *Nat. Struct. Mol. Biol.*, **16**, 1259–1266.

43. Yoda, M., Kawamata, T., Paroo, Z., Ye, X., Iwasaki, S., Liu, Q. and Tomari, Y. (2010) ATP-dependent human RISC assembly pathways. *Nat. Struct. Mol. Biol.*, **17**, 17–23.
44. Matranga, C., Tomari, Y., Shin, C., Bartel, D.P. and Zamore, P.D. (2005) Passenger-strand cleavage facilitates assembly of siRNA into Ago2-containing RNAi enzyme complexes. *Cell*, **123**, 607–620.
45. Rand, T.A., Petersen, S., Du, F. and Wang, X. (2005) Argonaute2 cleaves the anti-guide strand of siRNA during RISC activation. *Cell*, **123**, 621–629.
46. Diederichs, S. and Haber, D.A. (2007) Dual role for argonautes in microRNA processing and posttranscriptional regulation of microRNA expression. *Cell*, **131**, 1097–1108.
47. Liu, Y., Ye, X., Jiang, F., Liang, C., Chen, D., Peng, J., Kinch, L.N., Grishin, N.V. and Liu, Q. (2009) C3PO, an endoribonuclease that promotes RNAi by facilitating RISC activation. *Science*, **325**, 750–753.
48. Tian, Y., Simanshu, D.K., Ascano, M., Diaz-Avalos, R., Park, A.Y., Juraneck, S.A., Rice, W.J., Yin, Q., Robinson, C.V., Tuschl, T. *et al.* (2011) Multimeric assembly and biochemical characterization of the Trax-translin endonuclease complex. *Nat. Struct. Mol. Biol.*, **18**, 658–664.
49. Petri, S., Dueck, A., Lehmann, G., Putz, N., Rudel, S., Kremmer, E. and Meister, G. (2011) Increased siRNA duplex stability correlates with reduced off-target and elevated on-target effects. *RNA*, **17**, 737–749.
50. Leuschner, P.J., Ameres, S.L., Kueng, S. and Martinez, J. (2006) Cleavage of the siRNA passenger strand during RISC assembly in human cells. *EMBO Rep.*, **7**, 314–320.
51. Miyoshi, K., Tsukumo, H., Nagami, T., Siomi, H. and Siomi, M.C. (2005) Slicer function of *Drosophila* Argonautes and its involvement in RISC formation. *Genes Dev.*, **19**, 2837–2848.
52. Kraynack, B.A. and Baker, B.F. (2006) Small interfering RNAs containing full 2'-O-methylribonucleotide-modified sense strands display Argonaute2/eIF2C2-dependent activity. *RNA*, **12**, 163–176.
53. Robb, G.B. and Rana, T.M. (2007) RNA helicase A interacts with RISC in human cells and functions in RISC loading. *Mol. Cell*, **26**, 523–537.
54. Bannasser, Y., Le, S.Y., Benkirane, M. and Jeang, K.T. (2005) Evidence that HIV-1 encodes an siRNA and a suppressor of RNA silencing. *Immunity*, **22**, 607–619.
55. Harborth, J., Elbashir, S.M., Vandeburgh, K., Manninga, H., Scaringe, S.A., Weber, K. and Tuschl, T. (2003) Sequence, chemical, and structural variation of small interfering RNAs and short hairpin RNAs and the effect on mammalian gene silencing. *Antisense Nucleic Acid Drug Dev.*, **13**, 83–105.
56. Vlassov, A.V., Korba, B., Farrar, K., Mukerjee, S., Seyhan, A.A., Ilves, H., Kaspar, R.L., Leake, D., Kazakov, S.A. and Johnston, B.H. (2007) shRNAs targeting hepatitis C: effects of sequence and structural features, and comparison with siRNA. *Oligonucleotides*, **17**, 223–236.
57. McManus, M.T., Petersen, C.P., Haines, B.B., Chen, J. and Sharp, P.A. (2002) Gene silencing using micro-RNA designed hairpins. *RNA*, **8**, 842–850.
58. McIntyre, G.J., Yu, Y.H., Lomas, M. and Fanning, G.C. (2011) The effects of stem length and core placement on shRNA activity. *BMC Mol. Biol.*, **12**, 34.
59. Kumar, P., Johnston, B.H. and Kazakov, S.A. (2011) miR-ID: a novel, circularization-based platform for detection of microRNAs. *RNA*, **17**, 365–380.
60. Ge, Q., Dallas, A., Ilves, H., Shorestein, J., Behlke, M.A. and Johnston, B.H. (2010) Effects of chemical modification on the potency, serum stability, and immunostimulatory properties of short shRNAs. *RNA*, **16**, 118–130.
61. Macrae, I.J., Zhou, K., Li, F., Repic, A., Brooks, A.N., Cande, W.Z., Adams, P.D. and Doudna, J.A. (2006) Structural basis for double-stranded RNA processing by Dicer. *Science*, **311**, 195–198.
62. Preall, J.B., He, Z., Gorra, J.M. and Sontheimer, E.J. (2006) Short interfering RNA strand selection is independent of dsRNA processing polarity during RNAi in *Drosophila*. *Curr. Biol.*, **16**, 530–535.
63. Schwarz, D.S., Hutvagner, G., Du, T., Xu, Z., Aronin, N. and Zamore, P.D. (2003) Asymmetry in the assembly of the RNAi enzyme complex. *Cell*, **115**, 199–208.
64. Tomari, Y., Matranga, C., Haley, B., Martinez, N. and Zamore, P.D. (2004) A protein sensor for siRNA asymmetry. *Science*, **306**, 1377–1380.
65. Suzuki, H.I., Arase, M., Matsuyama, H., Choi, Y.L., Ueno, T., Mano, H., Sugimoto, K. and Miyazono, K. (2011) MCPIP1 ribonuclease antagonizes dicer and terminates microRNA biogenesis through precursor microRNA degradation. *Mol. Cell*, **44**, 424–436.
66. Woese, C.R., Winker, S. and Gutell, R.R. (1990) Architecture of ribosomal RNA: constraints on the sequence of 'tetra-loops'. *Proc. Natl Acad. Sci. USA*, **87**, 8467–8471.
67. Jucker, F.M. and Pardi, A. (1995) Solution structure of the CUUG hairpin loop: a novel RNA tetraloop motif. *Biochemistry*, **34**, 14416–14427.
68. Pei, Y., Hancock, P.J., Zhang, H., Bartz, R., Cherrin, C., Innocent, N., Pomerantz, C.J., Seitzer, J., Koser, M.L., Abrams, M.T. *et al.* (2010) Quantitative evaluation of siRNA delivery in vivo. *RNA*, **16**, 2553–2563.
69. Boland, A., Huntzinger, E., Schmidt, S., Izaurralde, E. and Weichenrieder, O. (2011) Crystal structure of the MID-PIWI lobe of a eukaryotic Argonaute protein. *Proc. Natl Acad. Sci. USA*, **108**, 10466–10471.

Supplemental Table S1. Sequences of siRNAs and sshRNAs

Name	Sequence	Name	Sequence
si19-3	5' -GCACGAAUCCUAAACCUCAU-3' 3' -UU CGUGCUUAGGAUUUGGAGU -5'	sh1	5' -GGGAGCACGAAUCCUAAACCUCAAAGA ^{C U U C} 3' -UU CUCGUGCUUAGGAUUUGGAGUUUCU _{A C U G}
SG68R	5' -GCACGAAUCCUAAACCUCA ^{C A} 3' -UU CGUGCUUAGGAUUUGGAGU _{A U}	SG68L	5' - UGAGGUUUAGGAUUCGUGC ^{C A} 3' -UUACUCCAAAUCCUAAGCAG _{A U}
SG72R	5' -GUGCACCAUGAGCACGAU ^{C A} 3' -UU CACGUGGUACUCGUGCUUA _{A U}	SG72L	5' - AUUCGUGCUC AUGGUGCAC ^{C A} 3' -UUUAAGCACGAGUACCACGUG _{A U}
SG74R	5' -CCUAAACCUCAAAGAAAA ^{C A} 3' -UU GGAUUUGGAGUUUCUUUUU _{A U}	SG74L	5' - UUUUUCUUUGAGGUUAGG ^{C A} 3' -UUAAAAAGAAACUCCAAAUC _{A U}
SG103(R)	5' -GUGCACCAUGAGCACGAU _U 3' -UU CACGUGGUACUCGUGCUUA _U	SG105(L)	5' - UGAGGUUUAGGAUUCGUGC _U 3' -ACUCCAAAUCCUAAGCAG _U
SG108(L)	5' - UUUUUCUUUGAGGUUAGG _U 3' -UUAAAAAGAAACUCCAAAUC _U	SG118(L)	5' - AUUCGUGCUC AUGGUGCAC _U 3' -UUUAAGCACGAGUACCACGUG _U
SG119(L)	5' - UGAGGUUUAGGAUUCGUGC - 3' -ACUCCAAAUCCUAAGCA	SG120(L)	5' - UGAGGUUUAGGAUUCGUGC - 3' -ACUCCAAAUC 
SG137(L)	5' - AUUCGUGCUC AUGGUGCAC _U 3' -UAAGCACGAGUACCACGUG _U	SG145(L)	5' - UGAGGUUUAGGAUUCGUGC _U 3' -ACUCCAAA GAAC AAGCAG _U
SG148(R)	5' -GCACGAA CAAG AAACCUCA ^{C A} 3' -UU CGUGCUUAGGAUUUGGAGU _{A U}	SG150(R)	5' -GCACGAAUCCUAAACCUCA _U 3' -UU CGUGCUUAGGAUUUGGAGU _U
SG151(R)	5' -GCACGAAUCCUAAACCU- 3' -UU CGUGCUUAGGAUUUGGAGU	SG159(R)	5' -CCUAAACCUCAAAGAAAA _U 3' -UU GGAUUUGGAGUUUCUUUUU _U
SG209(L)	5' - UGAGGUUUAGGAUUCGUGC _t 3' -ACUCCAAAUCCUAAGCAC _g	SG210(L)	5' - UGAGGUUUAGGAUUCGUGC *c* _{t*} 3' -ACUCCAAAUCCUAAGCAC*g* _t
SG214(L)	5' - UGAGGUUUAGGAUUCGUGC _U 3' -ACUCCAAAU* C*C *UAAGCAG _U	SG222(L)	5' - UGAGGUUUAGGAUUCGUGC _U 3' -ACUCCAAAU C*mC UAAGCAG _U
SG224(L)	5' - UGAGGUUUAGGAUUCGUGC _U 3' - ACUCCAAAUCCUAAGCAG _U	SG227(L)	5' - UGAGGUUUAGGAUUCGUGC _U 3' -actccaaatcctaagcag _U
SG229(L)	5' - UGAGGUUUAGGAUUCGUGC _{C3} 3' -ACUCCAAAUCCUAAGCAG _{C3}	SG230(R)	5' -GCACGAAU C *CUAAACCUCA ^{C A} 3' -UU CGUGCUUAGGAUUUGGAGU _{A U}
SG234(R)	5' -GCACGAAUCCUAAACCUCA ^{C*} _{a*} 3' -UU CGUGCUUAGGAUUUGGAGU * _{a*} _{a*}	SG237(L)	5' - AUUCGUGCUC AUGGUGCAC _U 3' -TTUA AGCACGAGUACCACGUG _U

SG244(L)	5' -UGAGGUUUAGGAUUCGUGC 3' -CUAAGCAG <u>CG</u> <u>U</u>	SG246(L)	5' -AUUCGUGCUC AUGGUGCAC <u>U</u> 3' -UAAGCAGAGUACCACGUG <u>U</u>
SG257(R)	5' -GCACGAAUCCUAAACCUC <u>A</u> <u>U</u> 3' -TT <u>CGUGCUUAGGAUUUGGAGU</u> <u>U</u>	SG221(C)	5' -CGUGCUUAGGAUUUGGAGU <u>U</u> 3' -GCACGAAUCCUAAACCUC <u>A</u> <u>U</u>

Red: guide strand; black: passenger strand, overhang, and loop/linker; pink: mismatch; blue: proposed slicer site. *: phosphorothioate bond; lower-case letters: DNA; m or underline: 2'-OMe modification. Although complementary sequences are aligned, no specific pairing of nucleotides near the loop is implied, as this feature was not specifically examined.

Supplemental Online Methods

Western blotting to measure Dicer turnover in Mouse Embryonic Fibroblast Cells

Immortalized MEFs were infected with Adeno-Cre Virus from the University of Iowa Gene Transfer Vector core with a titer of 6×10^{10} pfu/ml (1×10^{13} pt/ml) for 24 hours. *Dicer^{flox/flox}*; Rosa-YFP and *Dicer^{flox/wt}*; Rosa-YFP cells were infected at an MOI of 144 and 90 respectively, to achieve over 99% recombination efficiency in these lines, as determined by genotyping and FACS for YFP.

For Dicer Western blotting analysis, infected cells were lysed at 0, 24, 48, 72, 96, 120, 144, and 168 hours post infection in RIPA buffer plus protease inhibitors and 25 ug of total protein was loaded into 4-12% Bis-Tris Gels with MOPS. Due to the large size of Dicer (218 kDa), traditional wet transfers were performed in 10% methanol for 2.5 hours on ice. The blots were probed with a Dicer rabbit polyclonal antibody from Santa Cruz (H-212) at 1:200.

RT-qPCR assay. Total RNA was isolated from CDK-MEFs that had been treated either with or without Adeno-Cre at day 7 using a Trizol kit (Life Technologies) according to the manufacturer's instructions. Expression analysis of miRNAs was performed using the miR-ID RT-qPCR method following the procedure and primers described in Kumar et al (59). Data were analyzed by the $\Delta\Delta C_t$ method.

In vitro Dicer cleavage assay

sshRNA (8 pmol) was incubated in a 10 μ L reaction in the presence of 1U of recombinant Dicer enzyme (Agilent Technology, Stratagene, Catalog #240100, La Jolla, CA) and buffer containing 150 mM NaCl, 20 mM Tris-HCl (pH 8), and 2.5 mM $MgCl_2$ for 18 hours at 37°C. Control reactions that contained each shRNA but lacked Dicer were incubated in parallel. Samples were analyzed by 10% non-denaturing PAGE with SYBR Gold staining.

Serum stability assay of L-sshRNAs and R-sshRNAs

sshRNAs (3.35 μ g) with and without 2'-OMe modifications were incubated with 10% human serum (Sigma-Aldrich, St Louis, MO) for various times (0', 5', 1h, 2h, 4h, 8h, and 24h) in PBS at 37°C. At each time point, an aliquot was taken out, mixed with 2X gel loading buffer (Ambion, Austin, TX), and immediately stored in -80°C. The samples were analyzed by 12% denaturing PAGE (12% polyacrylamide, 20% formamide, and 8M urea) and were stained with SYBR Gold (Invitrogen, Carlsbad, CA).

Supplemental Online Figure Legends

Figure S1. Confirmation of Dicer ablation and Dicer turnover in Mouse Embryonic Fibroblast Cells.

(A) FACS analysis of YFP expression in *dicer*^{+/+} MEFs (top) and *dicer*^{-/-} MEFs 7 days after treatment with Adeno-Cre virus to induce recombination (bottom). Statistical analysis indicates a recombination level of 95% by day 7. (B) Western blotting of Dicer protein following removal of *Dicer*^{fllox/fllox} with Adeno-Cre virus at 0, 24, 48, 72, 96, 120, 144, and 168 hours post treatment shown with tubulin loading control.

(C) Comparison of levels of miRNA expression between Dicer knockout at day 7 (*dicer*^{-/-}) and wt Dicer-MEFs (*dicer*^{+/+}) measured by RT-qPCR assay (miR-ID method)(58) shows that miRNAs are depleted from the *dicer*^{-/-} MEFs cells by 80-90%.

Figure S2. Comparison of in vitro Dicer cleavage of 2'-OMe-modified sshRNAs (SG224L) vs. unmodified sshRNAs (SG105L) in their dimeric forms. (A) sshRNAs with (*) or without heating and snap cooling were subjected to recombinant Dicer treatment as indicated (lanes labeled +). Control reactions that contained each shRNA but lacked Dicer were incubated in parallel. Samples were analyzed by 10% non-denaturing PAGE with SYBR Gold staining. (B) Sequences and predicted secondary structures of monomeric and dimeric forms of L-sshRNAs. Red (guide strand sequences), Black (passenger strand sequences), and blue (linker sequences). Underlined bases indicate the presence of a 2'OMe-modification.

Figure S3. Comparison of L and R-sshRNAs with various loop sizes and chemical modifications. sshRNAs against the same target were compared for their ability to suppress the expression of the HCV IRES/fLuc reporter in 293FT cells. The sshRNAs were cotransfected in triplicate with the reporter DNA. (A) Effect of non-nucleotidic loops on activity of L-sshRNAs. (B) Effect of loop size on R-sshRNA activity.

Figure S4. Serum stability assay of L-sshRNAs and R-sshRNAs

sshRNAs (3.35 µg) with and without 2'-OMe modifications were incubated with 10% human serum (Sigma-Aldrich, St Louis, MO) for various times in PBS at 37°C. At each time point, an aliquot was taken out, mixed with 2X gel loading buffer (Ambion, Austin, TX), and immediately stored in -80°C. The samples were analyzed by 12% denaturing PAGE (12% polyacrylamide, 20% formamide, and 8M urea) and were stained with SYBR Gold (Invitrogen, Carlsbad, CA). Sequences and predicted secondary structures are depicted below the gels. Red (guide strand), Black (passenger strand), underlined bases (2'-OMe modification). (A) Analysis of R-sshRNAs. (B) Analysis of L-sshRNAs

Figure S5. Co-immunoprecipitation of L-sshRNAs targeting an additional site show Ago2-associated bands consistent with cleavage at the passenger strand slicer site. Denaturing PAGE analysis of L-sshRNAs isolated from Ago2 antibody-bound complexes that were 5'-end-labeled prior to transfection in 293FT cells (lanes SG237-Ago2, SG137-Ago2, SG246-Ago2). Full-length 5'-end-labeled sshRNAs were loaded as markers alongside the RNA that co-immunoprecipitated with hAgo2.

Because of the high T_m of the duplex of these sshRNAs, the full-length molecules were incompletely denatured under the electrophoresis conditions and thus migrate as two species. Gel bands labeled PS correspond to cleavage of sshRNA at the Passenger Strand slicer site. The slicer sites are marked by arrows on the sequences of the sshRNAs listed to the right of the gel.

Figure S6. Influence of target on strand selection for mature RISC. Top: Diagram of psiCHECKTM-2-pIRES construct used to evaluate targeting. A fragment of the HCV IRES containing the targets for a series of sshRNAs was inserted into the 3' UTR of *Renilla* luciferase in either forward or reverse orientation. The plasmid with the forward insert (pSG229) constituted the “sense” target, and the plasmid with the reversed insert (pSG230) became the “antisense” target, which could only be targeted by use of the “wrong” strand of the sshRNA (3' half in the case of L hairpins and 5' half in the case of R hairpins). The *Renilla* luciferase and firefly luciferase were driven by SV40 and HSV-TK promoters, respectively. The three target sites examined (68, 72, and 74) are shown as horizontal bars.

Bottom: The series of sshRNAs targeting sites 72 and 74 were synthesized with 5-nt and 2-nt loops in both L and R forms and tested for ability to suppress *Renilla* luciferase expression by cotransfecting them with psiCHECKTM-2-pIRES reporter plasmids into 293FT cells. Triplicate transfections were performed using a range of sshRNA concentrations, and *Renilla* luciferase expression level was normalized to the level of *firefly* luciferase expression to generate the dose response curves shown. The parent plasmid psiCHECKTM-2 was used as a negative control and showed no effect on *Renilla* luciferase expression (not shown).

Figure S7. Passenger strand slicing of SG224 is not dependent on the presence of target RNA. 5'-end-labeled and 3'-end-labeled sshRNAs were co-transfected in 293FT cells with one of the following target plasmids: pSG154 (perfect match target), pSG229 (short target sequence, complementary), pSG230 (short target sequence, antisense direction), or no target plasmid. Lysed cells were incubated with hAgo2 antibodies, and the isolated RNAs from these complexes were analyzed by denaturing gel electrophoresis.

Figure S8. Comparison of the efficacy and internal stability of R- and L-sshRNAs. (A-C) Comparison of silencing activity of R- and L-sshRNAs. Three sshRNAs (sh68, sh72, and sh74) were chemically synthesized with right- and left-hand loops. These sshRNAs were cotransfected in triplicate in a range of concentrations into 293FT cells with IRES/fLuc reporter plasmid (plasmid construct is shown in Fig. 1D). The *firefly* luciferase expression was measured 48 hours post-transfection. The experiments were repeated more than 3 times. (D-F) Comparison of internal stability of the 5' strands (19-nt) of the sshRNAs with right- and left-hand loop. Oligo 4.0 was used for the calculations without taking into account of the loop's impact on the internal stability of the 3' end of the strands. Solid triangle: R-sshRNA; open square: L-sshRNA; cross: siRNA.

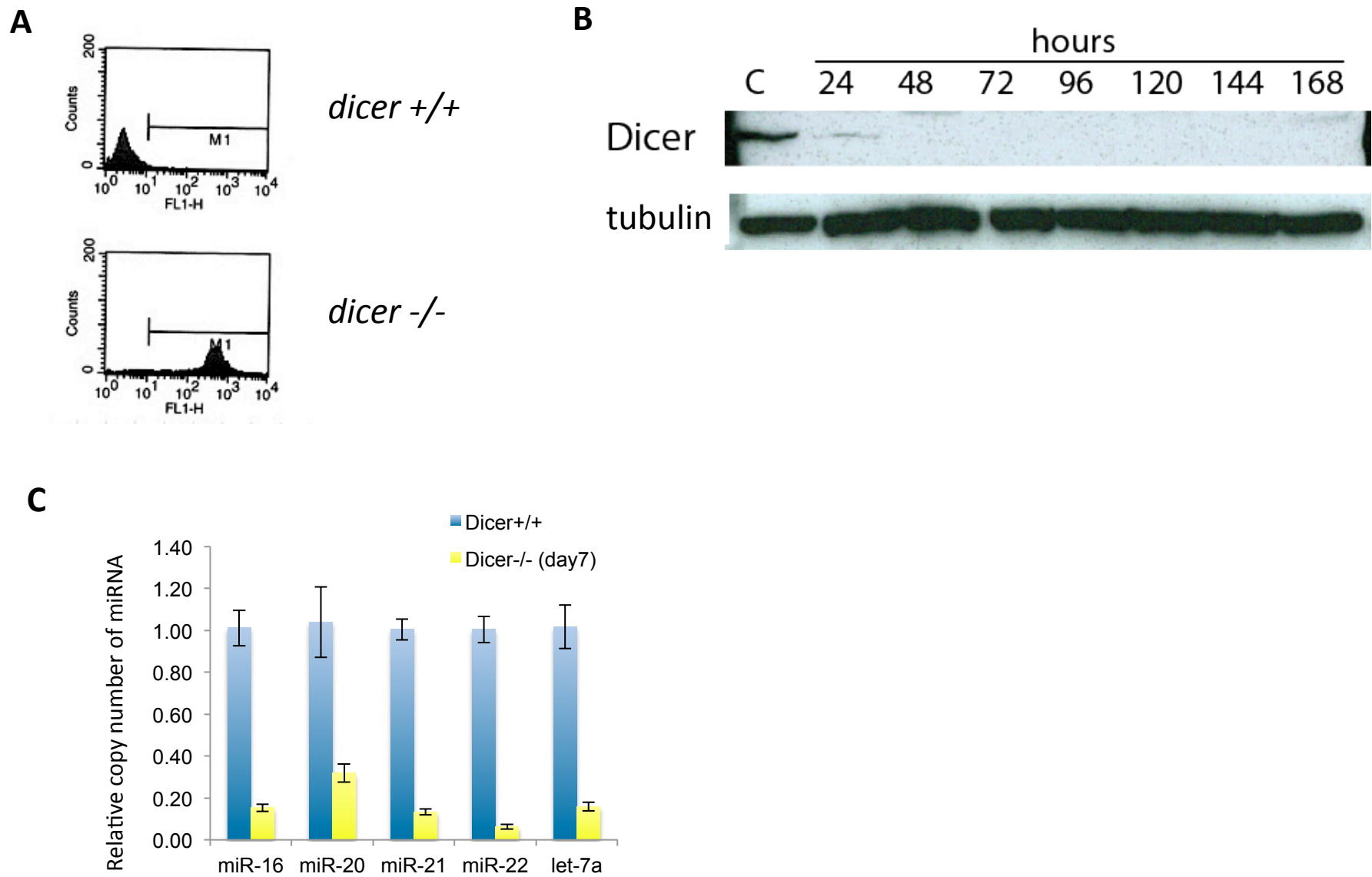


Figure S1

Non-denaturing PAGE analysis of in vitro Dicer reactions of SG105(L) and 2'OMe-modified SG224

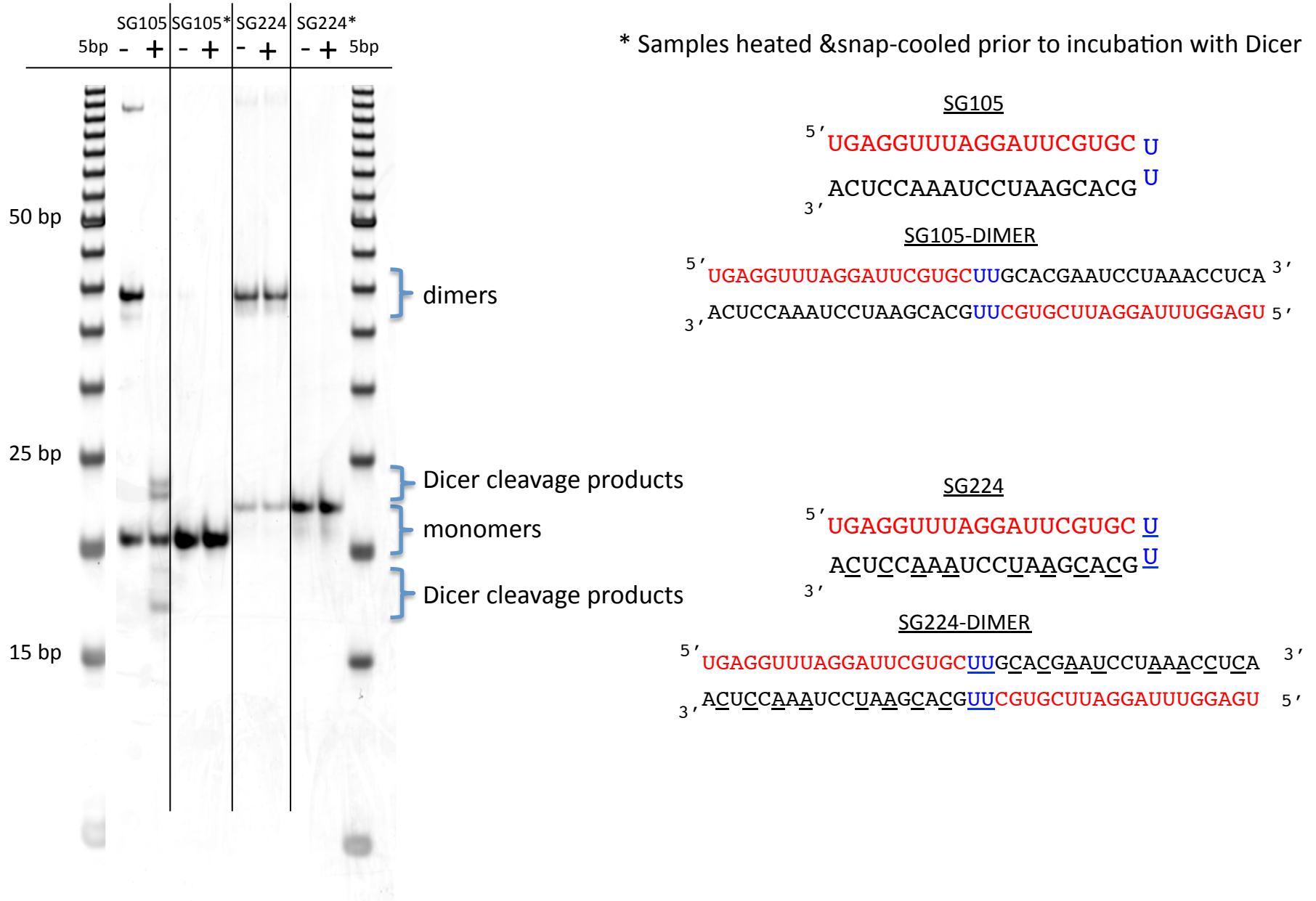
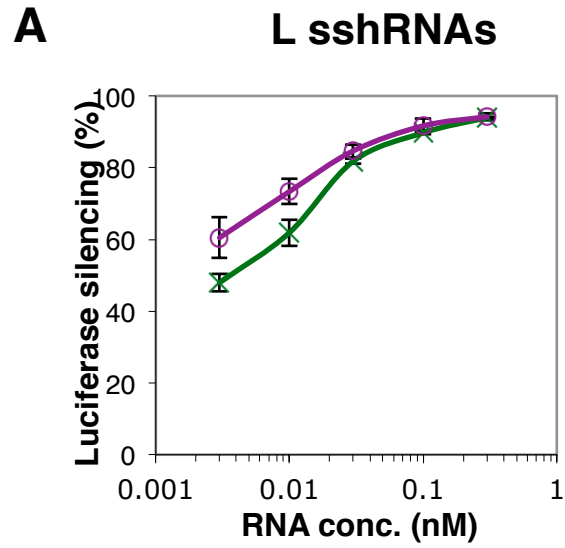
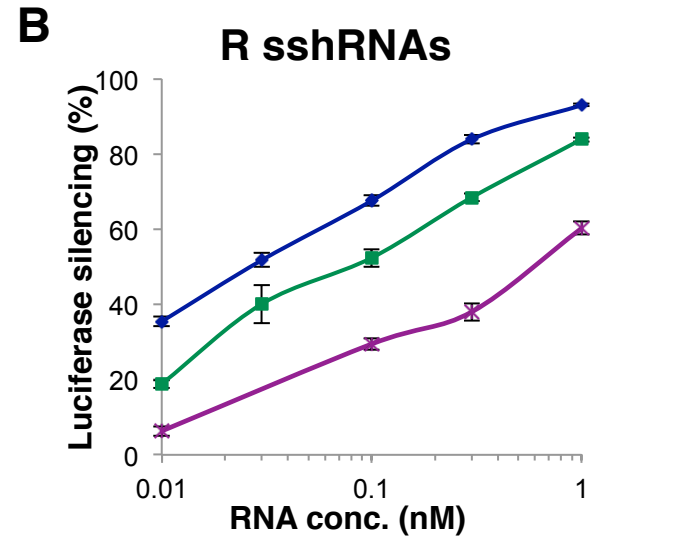


Figure S2



—*— SG105(L) (unmodified)
 —○— SG229(L) (loop: C3C3)



—◆— SG68(R) (unmodified, 5nt loop)
 —■— SG150(R) (unmodified, 2 nt loop)
 —×— SG257(R) (2'OMe, 2 nt loop)

Figure S3

A

Serum stability of R-sshRNAs

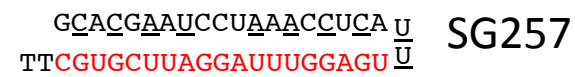
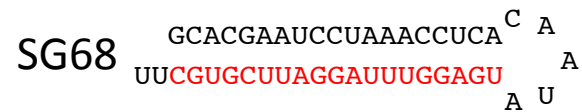
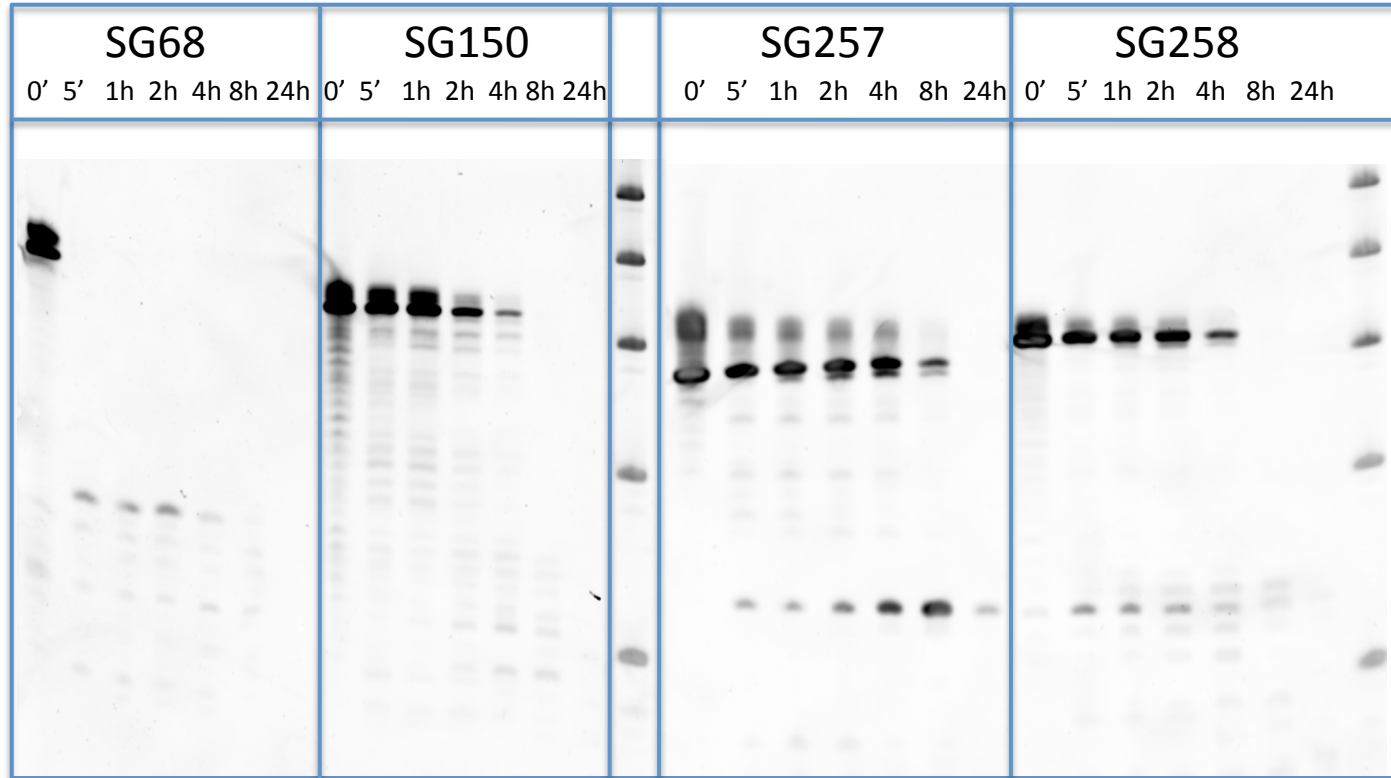
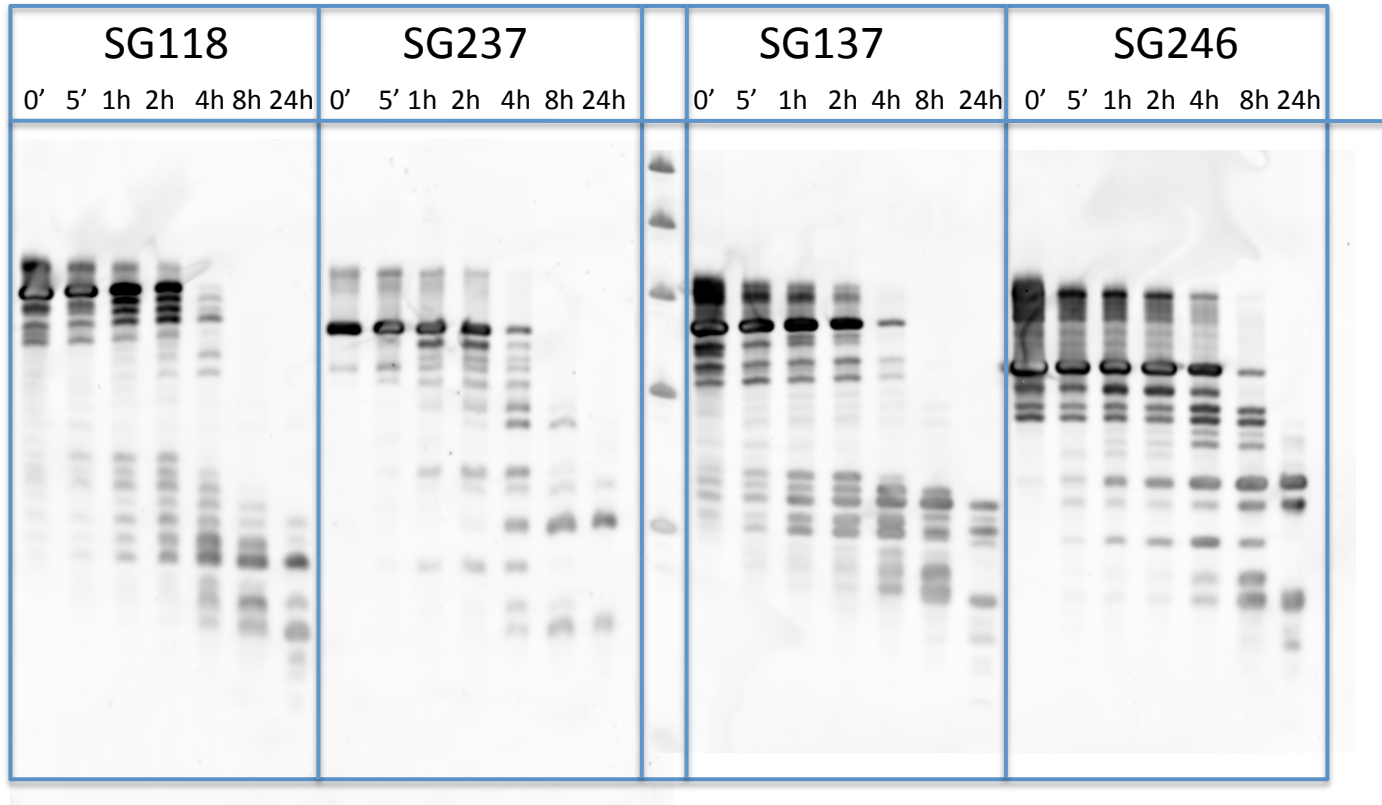


Figure S4A

B

Serum stability of L-sshRNAs



SG118 5' - **AUUCGUGCUC**AUGGUGCAC U
 3' - UUUAAGCAGAGUACCACGUG U

SG137 5' - **AUUCGUGCUC**AUGGUGCAC U
 3' - UAAGCAGAGUACCACGUG U

SG237 5' - **AUUCGUGCUC**AUGGUGCAC U
 3' - TTUAAGCAGAGUACCACGUG U

SG246 5' - **AUUCGUGCUC**AUGGUGCAC U
 3' - UAAGCAGAGUACCACGUG U

Figure S4B

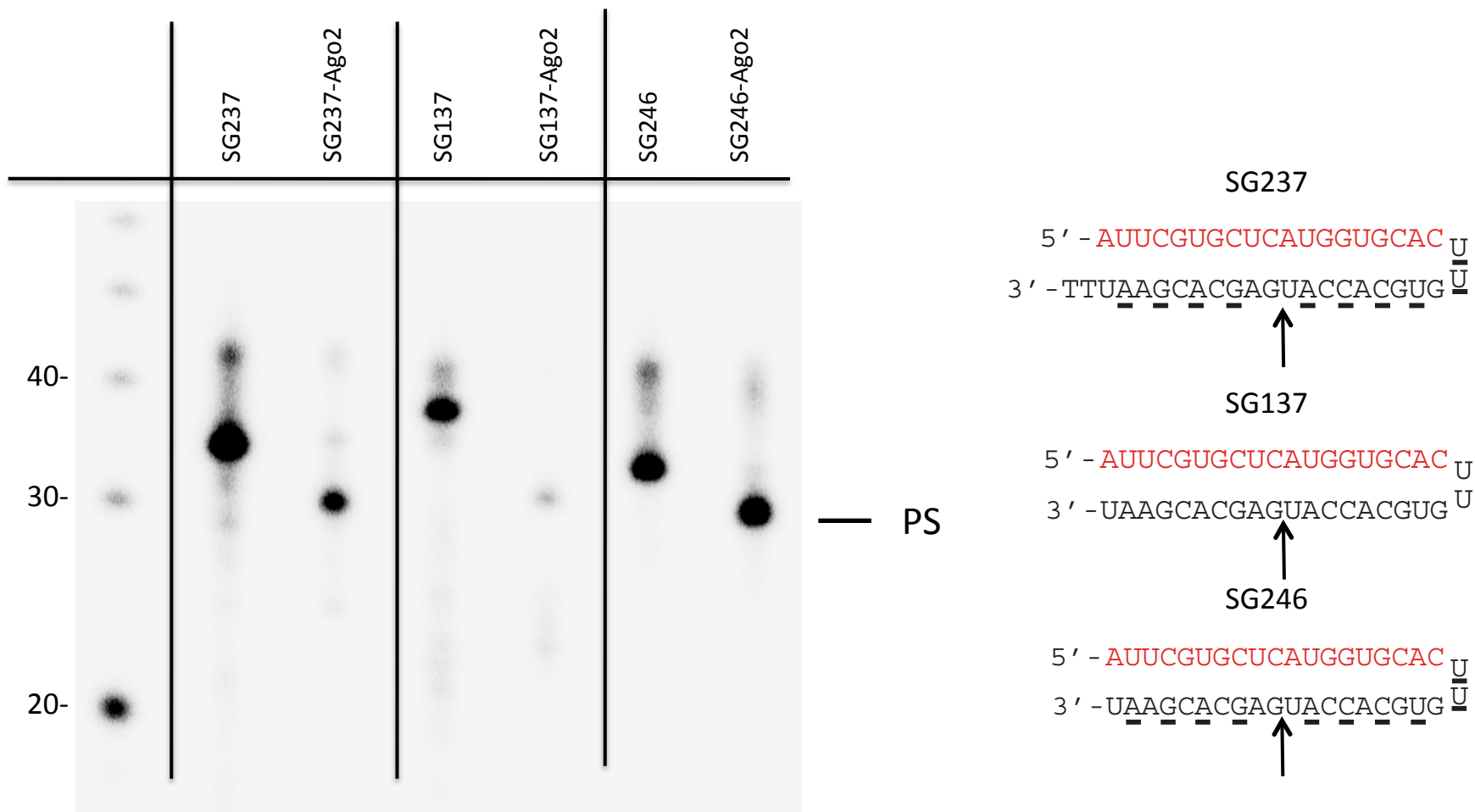
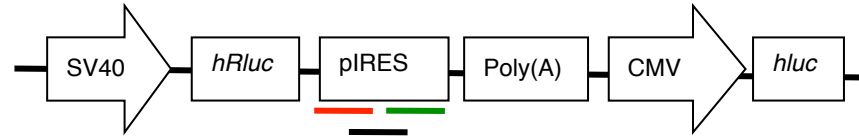
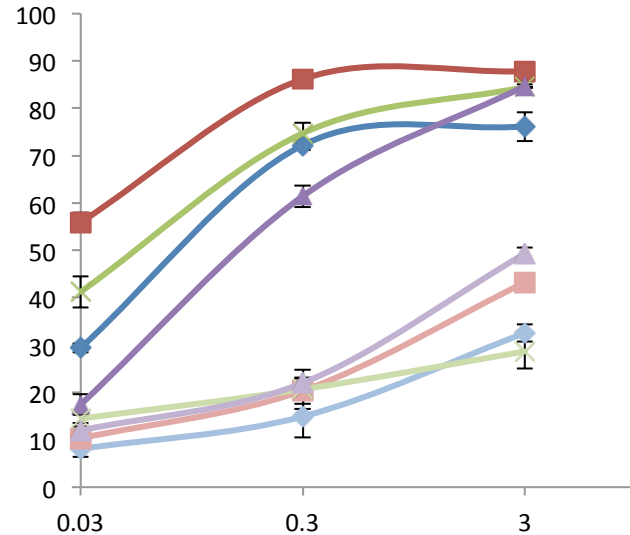


Figure S5

psiCHECK™-2-pIRES



72 series

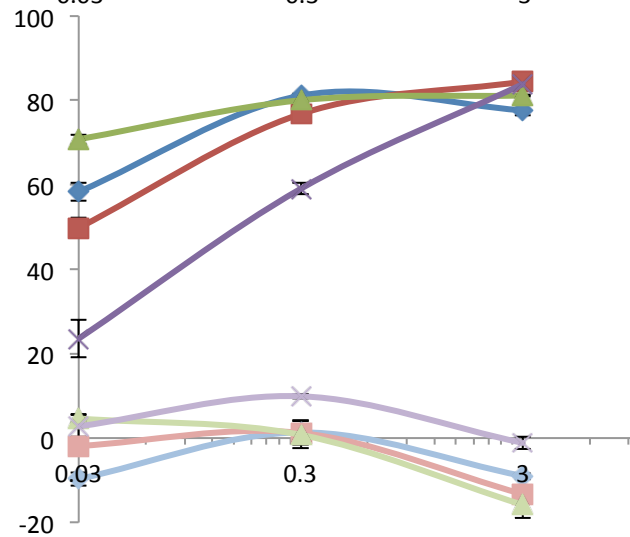


- SG72L-pSG229 (L, 5 nt loop)
- SG72R-pSG229 (R, 5 nt loop)
- SG118-pSG229 (L, 2 nt loop)
- SG103-pSG229 (R, 2 nt loop)
- SG72L-pSG230 (L, 5 nt loop)
- SG72R-pSG230 (R, 5 nt loop)
- SG118-pSG230 (L, 2 nt loop)
- SG103-pSG230 (R, 2 nt loop)

ON-target

OFF-target

74 series



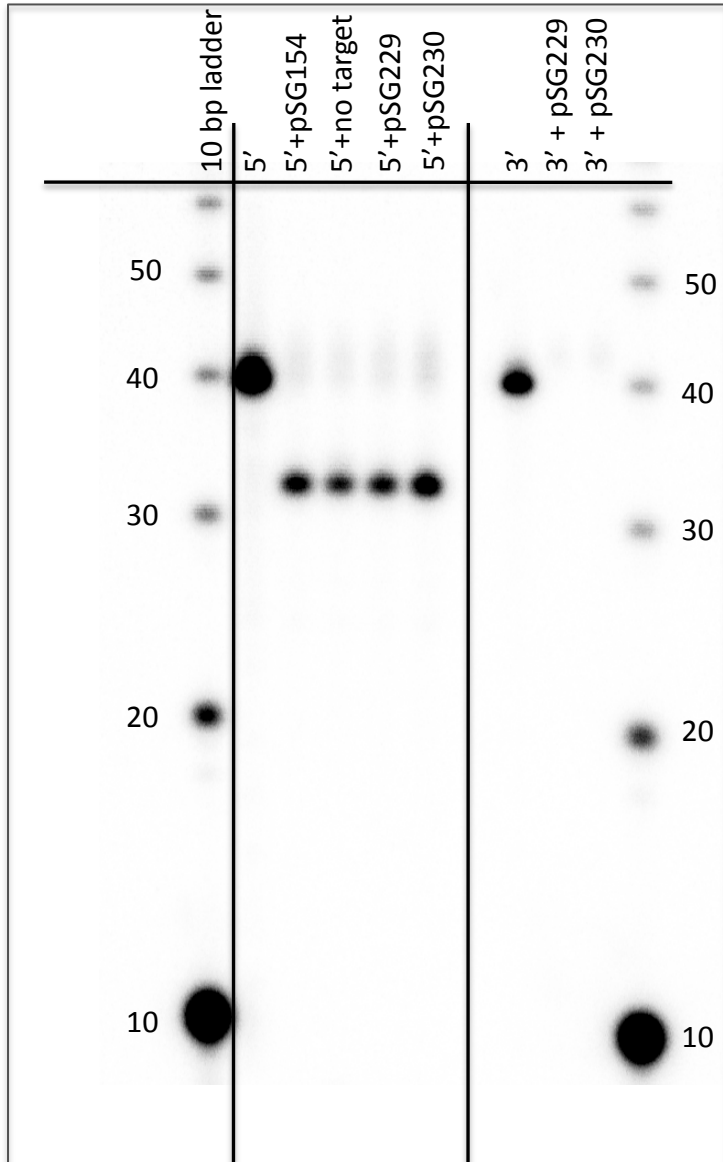
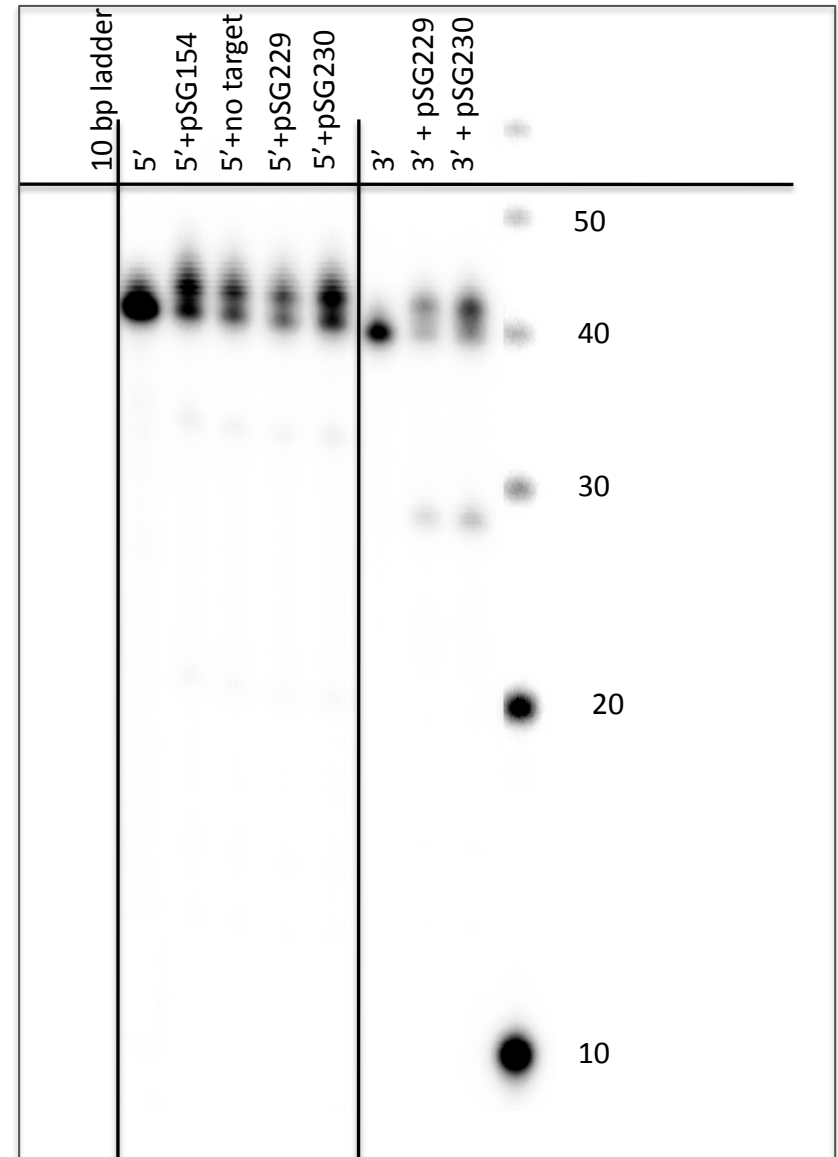
- SG74L-pSG229 (L, 5 nt loop)
- SG74R-pSG229 (R, 5 nt loop)
- SG108-pSG229 (L, 2 nt loop)
- SG159-pSG229 (R, 2 nt loop)
- SG74L-pSG230 (L, 5 nt loop)
- SG74R-pSG230 (R, 5 nt loop)
- SG108-pSG230 (L, 2 nt loop)
- SG159-pSG230 (R, 2 nt loop)

ON-target

OFF-target

pSG229: ON-TARGET vector
pSG230: OFF-TARGET vector

Figure S6

A**Ago2-associated fraction****B****Unbound fraction**

5' = 5'-end-labeled SG224
 3' = 3'-end-labeled SG224

Figure S7

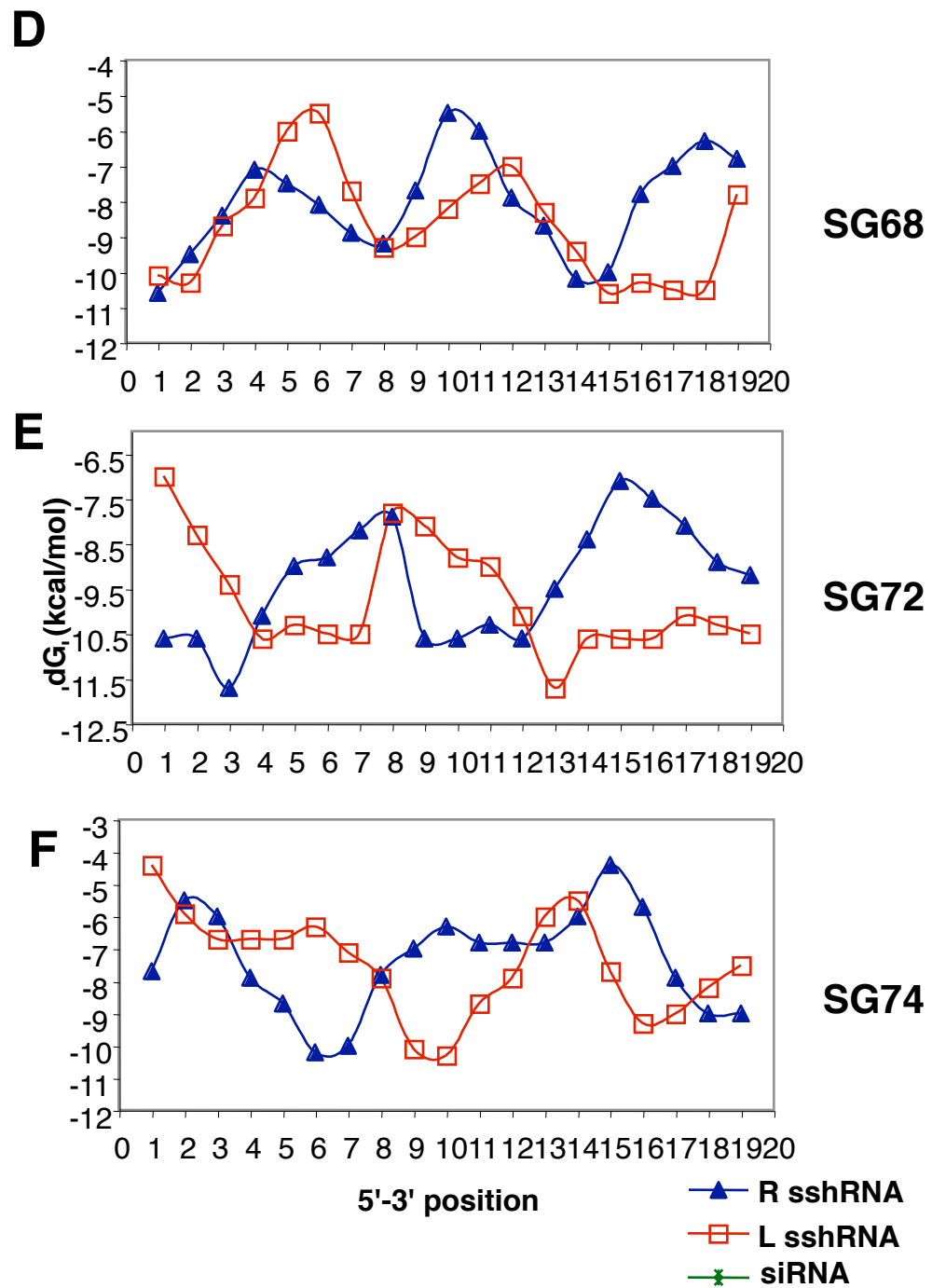
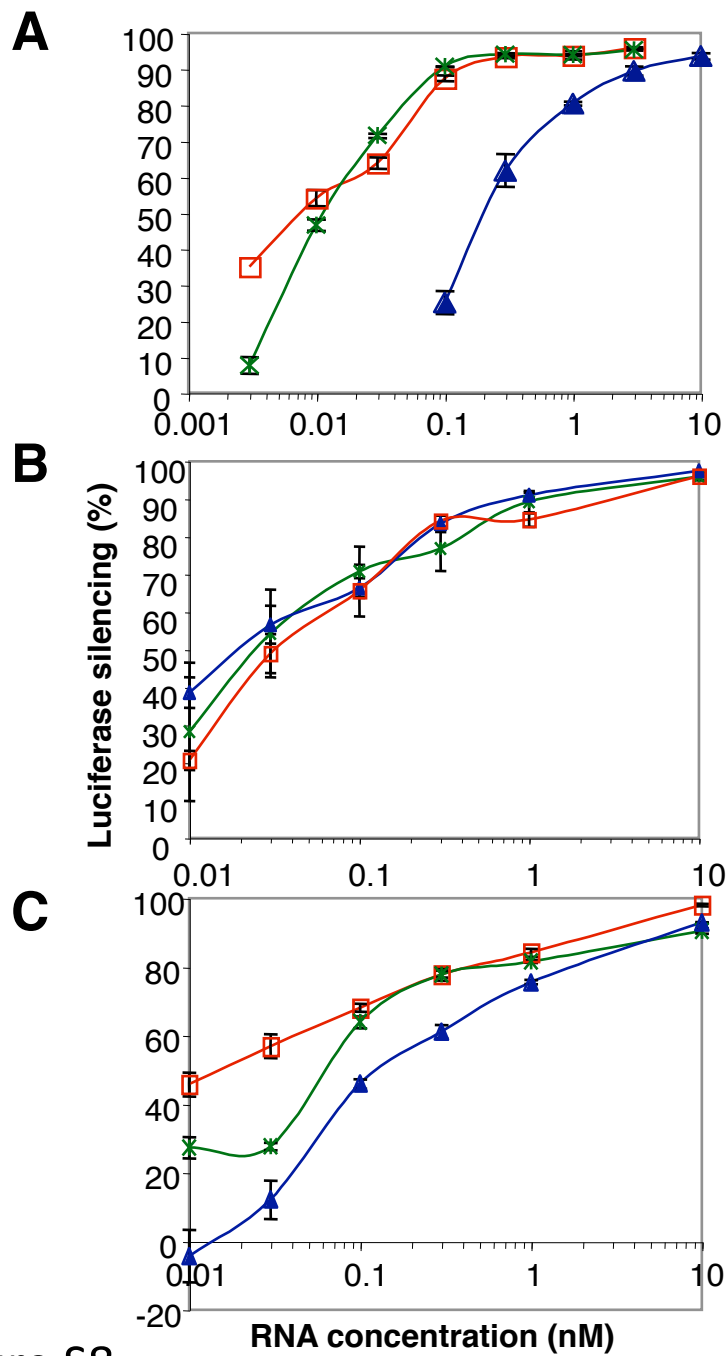


Figure S8